Vapor Transport Techniques for Growing Macroscopically Uniform Zinc Oxide Nanowires

by

Chad Allan Baker, B.S.

Thesis

Presented to the Faculty of the Graduate School of

The University of Texas at Austin

in Partial Fulfillment

of the Requirements

for the Degree of

Master of Science in Engineering

The University of Texas at Austin

August 2009

Vapor Transport Techniques for Growing Macroscopically Uniform Zinc Oxide Nanowires

Approved by
Supervising Committee:
Matthew Hall

Li Shi

Dedication

To: my loving fiancé, Kerrie, for all she has taught me about catalysis and for putting up with my stubbornness; my parents for encouraging me in my education.

Acknowledgements

I would like to thank Dr. Hall and Dr. Shi for advising me on this work and bearing with me through all the pitfalls associated with learning something as complicated as nanomaterial synthesis. I'd also like to thank Josh Carter, Jan-Michael Cabrera, Bridge Mellichamp, and Katherine Aristazabal. Their efforts made these results possible.

August 13, 2009

Abstract

Vapor Transport Techniques for Growing Macroscopically Uniform Zinc Oxide Nanowires

Chad Allan Baker, M.S.E.

The University of Texas at Austin, 2009

Supervisor: Matthew Hall

ZnO nanowires were grown using carbothermal reduction and convective vapor phase transport in a tube furnace. Si <100> substrates that were 20 mm x 76.2 mm were sputter coated with 2 nm to 50 nm gold which formed nanoparticles on the order of 50 nm in diameter through a process of Ostwald ripening upon being heated. Growth temperatures were varied from 800ºC to 1000ºC, flow rates were varied from 24 sccm to 3300 sccm, and growth durations were varied from 8 minutes to 5 hours. Vapor phase Zn, CO, and CO_2, produced by carbothermal reduction and suspended in an Ar atmosphere, were flowed over the Si substrates. The Au nanoparticles formed an eutectic alloy with Zn, causing them to become liquid nanodroplets which catalyzed vapor-liquid-solid nanowire growth. The nanowires were also synthesized by self-catalyzing vapor-solid growth in some cases. Using the tube furnace never resulted in more than 50% of the substrate being covered by nanowires. It was found that a bench-top furnace could

achieve nearly 100% nanowire coverage by placing the 20 mm x 76.2 mm sample face down in a quartz boat less than 2 mm above the source powder. This was because minimizing the distance between the sample and the source powder was critical to achieve macroscopically uniform growth consistently.

Table of Contents

List of Tables

List of Figures

Chapter 1: Introduction

Nanowires are nanoscopic cylindrical structures with diameters under 1 μm and lengths greater than 1 μm. Particularly, ZnO nanowires are nanowires synthesized in the favored <0001> direction, usually on the order of 20 nm to 150 nm in diameter, and up to tens of microns in length (Yang, et al. 2002). This research is unique in that the focus is on large scale, high areal density production of ZnO nanowires. Here, large scale means a surface area of roughly 15 cm^2, which has not been reported in the literature.

1.1 Motivation of This Research

This research is motivated by a desire to improve catalysts for reducing combustion emissions from internal combustion engines. Hydrocarbon and CO emissions are reduced by oxidation, and NO_x emissions are reduced by dissociation. ZnO nanowires will function as a high surface area substrate for catalytic metals. We expect that ZnO nanowires will potentially be effective in this role because of the high specific area and rugosity. Specific area is area per unit mass, and rugosity is actual surface area divided by nominal or projected surface area.

A typical conventional catalyst consists of a honeycomb ceramic structure with roughly 1mm x 1mm channels, the surfaces of which contain microscopic pores. A washcoat is used to apply the catalytic metals to the surfaces inside the channels and pores (Heck and Farrauto 2002). An apparent disadvantage of this configuration is that the catalytic activity sites are not distributed in such a way that all of the catalytic metal is equally utilized. This is the case because an exhaust gas molecule travels in a straight path until a collision occurs so the edge of a catalyst pore can produce a shadowing effect, preventing an exhaust gas molecule from reaching catalytic activity sites unless a molecule is on a path almost directly parallel to the catalyst pore. Figure 1.1 shows a

schematic of a traditional ceramic honeycomb catalyst. The small gray circles represent catalytic activity sites, and the arrows demonstrate the maximum possible angle of the path which a gas molecule must travel to reach a particular catalytic activity site.

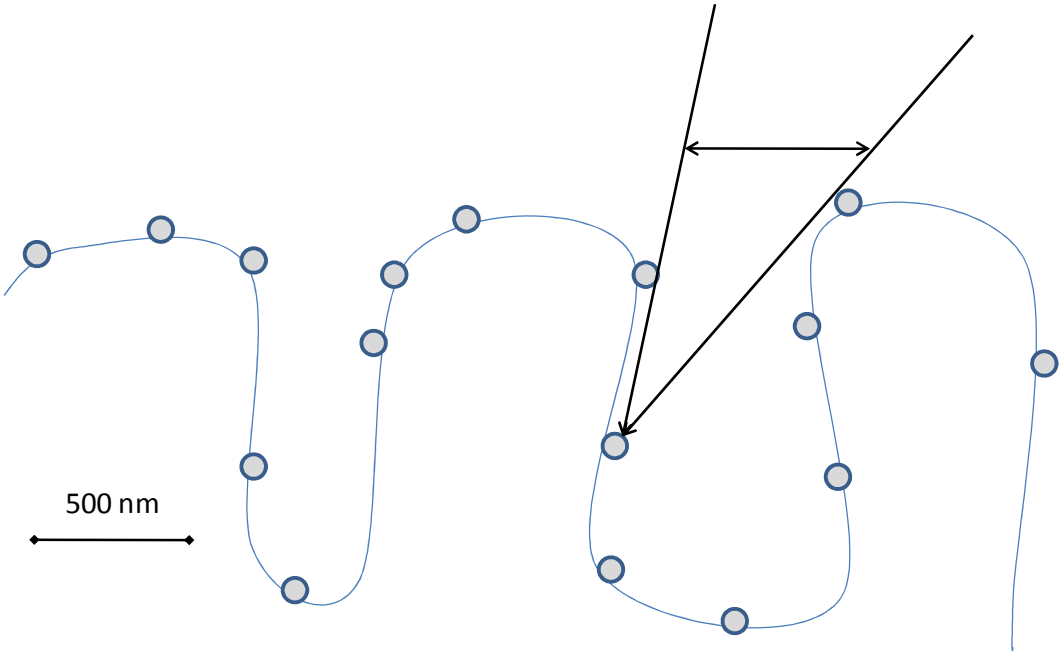

Figure 1.1: Schematic of conventional catalyst pores. Arrows show maximum angle for path of gas molecule that will collide with a particular catalyst site. Scale bar is for typical pore size.

As can be seen in the figure, the depth and aspect ratio of the pores affect the distance gas molecules can travel into the pore without changing direction. Because of this, Pt catalyst activity sites at the bottom of a pore cannot be as effectively used as catalyst activity sites at the mouth of a pore. A pore has a self-shadowing effect whereby the mouth of the pore shadows catalyst activity sites within that pore.

A nanowire offers a potential solution to this problem because a structure that protrudes outward from a substrate's surface does not shadow any of the Pt catalyst activity sites that are attached to that structure. In other words, there is no self-shadowing

effect caused by a nanowire. A schematic of what the nanowire is expected to look like is shown in Figure 1.2.

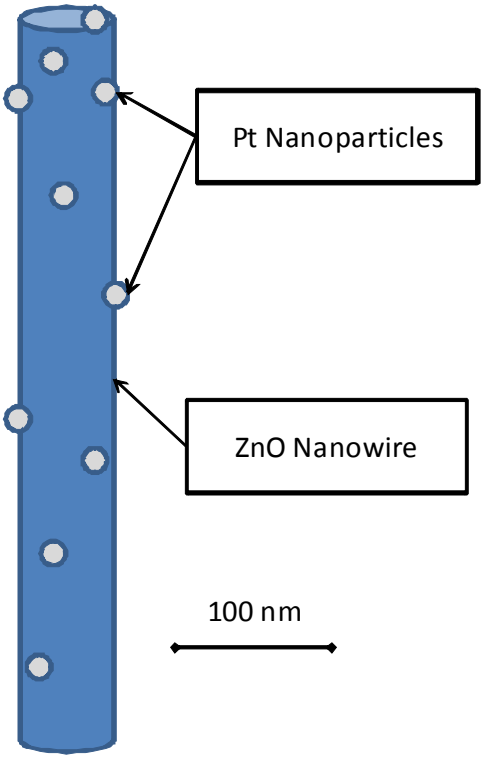

Figure 1.2: Schematic of ZnO nanowire covered with Pt nanoparticles. Scale bar is for typical ZnO nanowire size.

1.2 Other Applications of Zinc Oxide Nanowires

ZnO nanowires are used in photonic devices, piezoelectric devices, and field effect transistors. Because of the photoluminescent properties of ZnO nanowires, researchers are hoping to use ZnO nanowires in the medical field to locate single cancer cells, and the piezoelectric properties may make ZnO nanowires useful as power generation devices that can convert small mechanical vibrations into voltage and electrical current where power is needed on the microscopic scale (Wang 2004).

1.3 Zinc Oxide Nanowire Growth Methods

ZnO nanowires are grown by vapor-phase transport, aqueous solution chemistry, and organic solution chemistry (Greene, et al. 2006, Huang, et al. 2001). Apparatus for heating the growth species include tube furnaces, bench top furnaces, and microwave ovens (Unalan, et al. 2008).

1.4 Vapor-Phase Transport Growth

There are three important components of vapor-phase transport growth: source vapor production, transport method, and catalytic mechanisms. In general, materials are evaporated to produce source vapors which are transported to a substrate coated with metal. The proceeding sections present a detailed discussion of this process within the framework of the three aspects mentioned above.

1.4.1 Source Vapor Production

Several methods of producing the vapor precursor for ZnO nanowires have been reported in literature. The most commonly used method is carbothermal synthesis where a homogeneous mixture of graphite and ZnO powders reacts, producing vapor species which are transported to substrates via diffusion or convection. The carbothermal

reaction produces Zn vapor, CO vapor, and CO_2 vapor. This reaction is reported to occur reversibly at 900ºC (Hejazi, Hosseini and Ghamsari 2008, Wang, Song and Wang 2007, Yang, et al. 2002).

Another method is direct thermal evaporation of Zn powder; however, this method requires the presence of a gaseous oxidizer, and the only oxidizer that has been reported for this technique in literature is pure O_2 (Tseng, et al. 2003, Park, et al. 2003).

1.4.2 Transport Method

Diffusion and convection transport are used for transporting the vapors to the substrate. The diffusion only method is carried out in a furnace that is open to the atmosphere. For the convection transport method, an inert carrier gas, usually Ar or sometimes N_2, is flowed through a tube furnace to mix with the nanowire producing species and transport them downstream to the substrate (Yao, Chan and Wang 2002, Huang, et al. 2001, Prete, Lovergine and Tapfer 2007). Variations on this method include the use of O_2 to act as a nanowire-producing reactant and the use of vacuum (Wang, Song and Wang 2007, Park, et al. 2003, Tseng, et al. 2003).

1.4.3 Catalysis Mechanism

Au is most commonly used for the catalyst (Huang, et al. 2001, Wang, Song and Wang 2007, Kumar, et al. 2008), but some authors have reported using no catalyst (Yao, Chan and Wang 2002) or Cu catalyzed growth (Li, Lee and Tseng 2003). Although the Au catalyst has been studied more thoroughly than any other method, there is disagreement concerning the physical mechanism that causes the growth of the ZnO nanowire. Most researchers report the vapor-liquid-solid (VLS) tip growth mechanism. Hejazi et al. have presented a graphical means of explaining this mechanism which is shown in Figure 1.3.

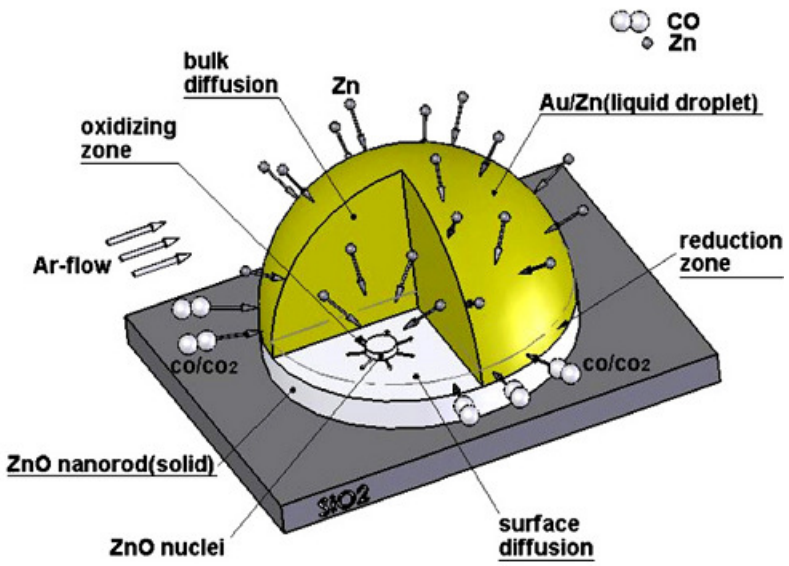

Figure 1.3: Schematic of VLS tip growth process. CO, CO_2, and Zn particles impinge on the Au nanodroplet, diffuse through the droplet, and react at the droplet-nanowire interface to form ZnO which aligns to form the nanowire. (Hejazi, Hosseini and Ghamsari 2008)

In the VLS process, a liquid nanodroplet at the tip of the nanowire catalyzes a reaction at the droplet-nanowire interface. This action pushes the droplet along at the tip of the nanowire as growth continues. Figure 1.3 shows reactant species impinging on the surface of the liquid Au nanodroplet, diffusing through to the interface between the nanodroplet and the newly forming nanowire, and reacting to cause growth of the nanowire.

Hejazi, Hosseini and Ghamsari (2008) claim that CO_2 and CO absorbed by the gold tip both contribute to nanowire growth by oxidizing absorbed Zn atoms. This contrasts with findings of Wang et al. which demonstrate that some small concentration of O_2 is necessary to allow the growth to happen. It is unclear from other literature whether oxygen is necessary for nanowire growth. Another group claims that ZnO vapor molecules can be formed either by oxidation of Zn in the gas phase or evaporated directly

from the source. These ZnO vapor molecules are adsorbed directly by the gold tip particle, eliminating the need for oxidizing surface reactions between adsorbed Zn atoms and an oxidizer (Kim, et al. 2008). It is also critical to note that this group uses the term particle rather than droplet when referring to the Au tip.

Another contradiction to the claims of Hejazi, Hosseini and Ghamsari (2008) is found in the results in catalyst literature about the oxidation of CO on Au surfaces. When adsorbed CO molecules and adsorbed O atoms react to form CO_2, the readsorption rate is so miniscule that it is not observed in experimental results. This means that CO_2 is almost never adsorbed by Au surfaces (Pansare, Sirijaruphan and Jr. 2005).

The catalytic metal can be applied as a thin film by sputter coating or thermal evaporation. Alternatively, nanoparticles can be spin coated onto the surface (Huang, et al. 2001). If the catalyst is applied as a thin film, when brought to the growth temperature, it will de-wet the substrate and form nanoparticles through a process known as Ostwald ripening (Voorhees 1985, Prete, Lovergine and Tapfer 2007).

For the VLS mechanism to occur, it is necessary for the Au to form a eutectic alloy with Zn so that the melting temperature drops to below the growth temperature and the solid nanoparticle becomes a liquid nanodroplet (Okamoto 2006). A binary Au-Zn phase diagram, which shows how melting temperature drops with increasing Zn concentration, is shown in Figure 1.4.

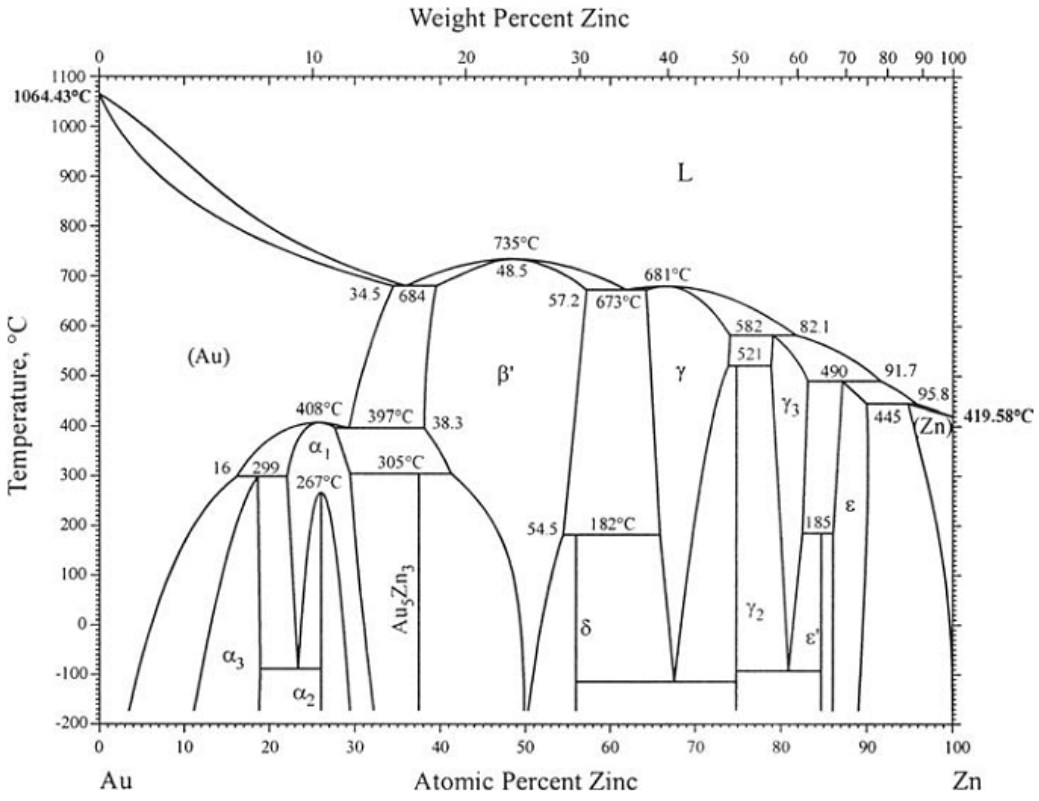

Figure 1.4: Binary gold-zinc phase diagram. (Okamoto 2006)

The melting point of bulk Au is 1064ºC (Okamoto 2006), and at the nanoscale this is somewhat reduced. However, for typical gold catalyst particle diameters on the order of 50 nm, the melting temperature is not reduced by more than a few degrees Celsius as shown in Figure 1.5 (Prete, Lovergine and Tapfer 2007, Buffat and Borel 1976). Noting that the abscissa of this figure has units of Angstroms, this establishes that it is impossible for the VLS mechanism to occur without the formation of an Au-Zn alloy for typical gold catalyst diameters reported in literature.

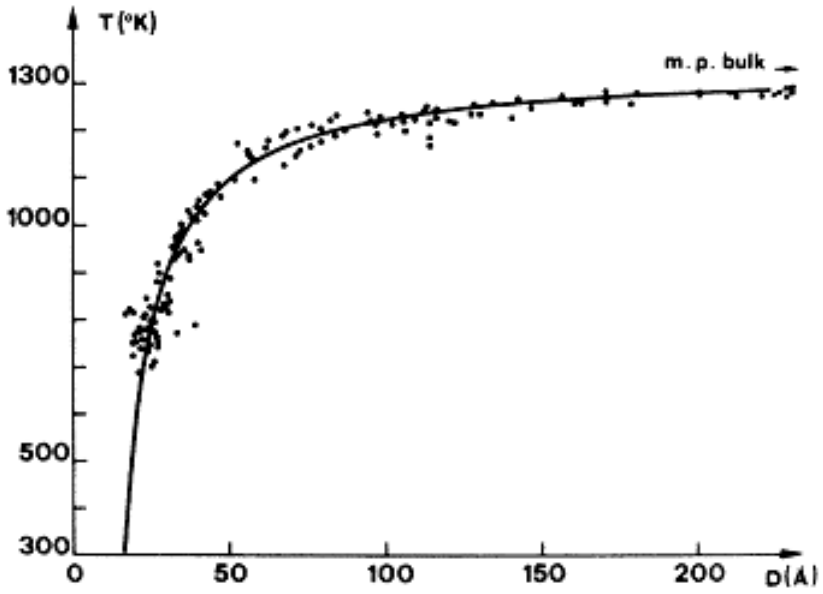

Figure 1.5: Experimental and theoretical values of melting temperature v. diameter for Au nanoparticles. (Buffat and Borel 1976)

Opponents of the VLS mechanism propose a vapor-solid-solid (VSS) or vapor-solid (VS) mechanism for the nanowire growth. One group has used in situ x-ray diffraction (XRD) analysis to demonstrate that the Au catalyst tips probably remain solid during nanowire growth at a synthesis temperature of 850ºC. During the growth, the XRD signature of Au remained present, indicating that the tips are neither melting nor alloying (Kirkham, et al. 2007). However, this claim is opposed by Kumar, et al. (2008) who performed extensive transmission electron microscopy (TEM) studies on grown nanowires over a range of temperatures. These studies have shown that the Au catalyst tip, at the resolution of a single nanowire, do not contain any Zn. However, Kumar et al. assert that Zn is likely precipitating out of the alloy solution and oxidizing as temperature is decreased from the growth temperature. This is a good explanation of why the Au tips are pure Au when observed after the growth. Moreover, Kumar et al. claim that authentic VLS growth occurs only in the 900ºC to 950ºC temperature range, which is above the

synthesis temperature of 850ºC reported by Kirkham et al. Kumar et al. also claim that VLS growth is characterized by unfaceted nanowires with diameters that are nearly identical to those of the Au tips. Faceted nanowires indicate growth by a VS mechanism in which ZnO is self catalyzed by the surfaces of the nanowire. Another group claims that tip growth does not occur for sufficiently high fluxes of ZnO vapor because the Au nanoparticle becomes saturated and cannot maintain function as a catalyst (Kim, et al. 2008). This is consistent with the claim that VS growth can produce nanowires with Au tips in some temperature ranges. These can be considered examples of VS growth because of their faceted appearance. Examples of each kind of growth are shown in the scanning electron microscope (SEM) image in Figure 1.6. Nanowires with no edges and a constant diameter are grown by the VLS mechanism, and faceted nanowires with edges that narrow near the tips are grown by the VS mechanism.

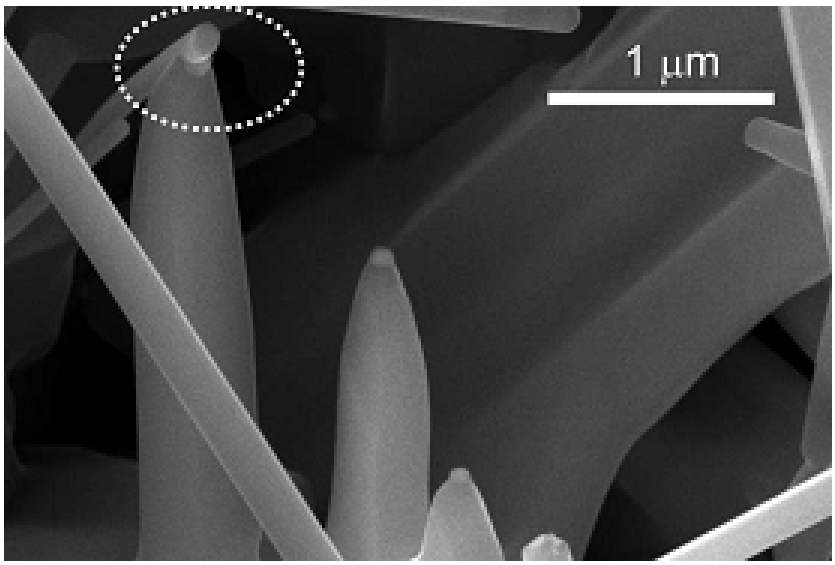

Figure 1.6: HR-SEM image showing examples of both VS growth and VLS growth. The circled region is the intersection of both types of nanowires. (Kumar, et al. 2008)

Chapter 2: Experimental Apparatus

2.1 Powder and Sample Preparation

In order to grow ZnO nanowires, a 20 mm by 76.2 mm Si sample must be prepared in order to provide a substrate, and ZnO powder and graphite powder must be mixed because these cannot be purchased premixed. After mixing, it is necessary to crush the powder to break up any agglomerations.

150 mm diameter by 650 μm thick <100> mech grade Si wafers, purchased from University Wafer, were cut using a Disco 321 Wafer Dicing Saw located in the 4th floor clean room in the Nanoscience and Technology (NST) Building at the University of Texas at Austin. Samples were sometimes cleaned with a sonicator using isopropanol, then ethanol, and finally deionized water in 500 mL beakers. To apply the catalyst metal, we used either the thermal evaporator in the fourth floor clean room of the NST Building or the RF sputter coater in the Institute for Cellular or Molecular Biology (ICMB) microscopy facility. A 99.99% pure gold filament and a tungsten heating element boat were used in the thermal evaporator, and a Ted Pella 0.1 mm 99.99% pure Au disk sputter target was used in the sputter coater. Recently, a Ted Pella 0.3 mm 99.99% pure Cu disk sputter target was also used. Both the thermal evaporator and the sputter coater had quartz crystal deposition thickness monitors. The sputter coater we used had not been calibrated correctly so all reported sputter coater values must be multiplied by 1.9 to obtain the actual thickness of the film that was deposited. Dwight Romanivicz, the ICMB microscopy facility scientist, used TEM to measure the thickness of a cross section of a layer of sputtered material that was 20 nm thick according to the quartz crystal deposition thickness monitor. According to TEM, the sputtered layer was 38 nm thick.

A triple beam balance was used to weigh graphite and ZnO powders. Kurt J. Lesker supplied the ZnO powder which was 200 mesh and 99.9% pure. The graphite powder was supplied by Sigma-Aldrich, and the analyis is shown in Table 2.1. The graphite powder is described as being fine, and no mesh size is given.

Soluble in ethanol	max. 0.2%
Loss on drying (120ºC)	max. 1%
Residue on ignition (1000ºC)	max. 1%

Table 2.1: Analysis results for graphite powder.

The powders were massed and stored in a 0.5 L Nalgene bottle, and the powder mixing was performed in a mortar and pestle.

2.2 TUBE FURNACE

Many experiments were carried out in a tube furnace set up, and gas flows were regulated with rotameters and a mass flow controller. The rotameters used were Cole Parmer model PMR1-010298 (referred to as Rotameter 98), Cole Parmer model PMR1-010290 (referred to as Rotmeter 90), and Expotech model G-03294-18 (referred to as Rotameter 18). An Aera FC-7800XCU electronic mass flow controller, shown in Figure 2.1, was used to regulate flows of 30 sccm or less. Gases used were Ar, CO_2, air, and 5% O_2 diluted with N_2 and Ar. The flow control device and gas used for each experiment is shown in Table A.1.

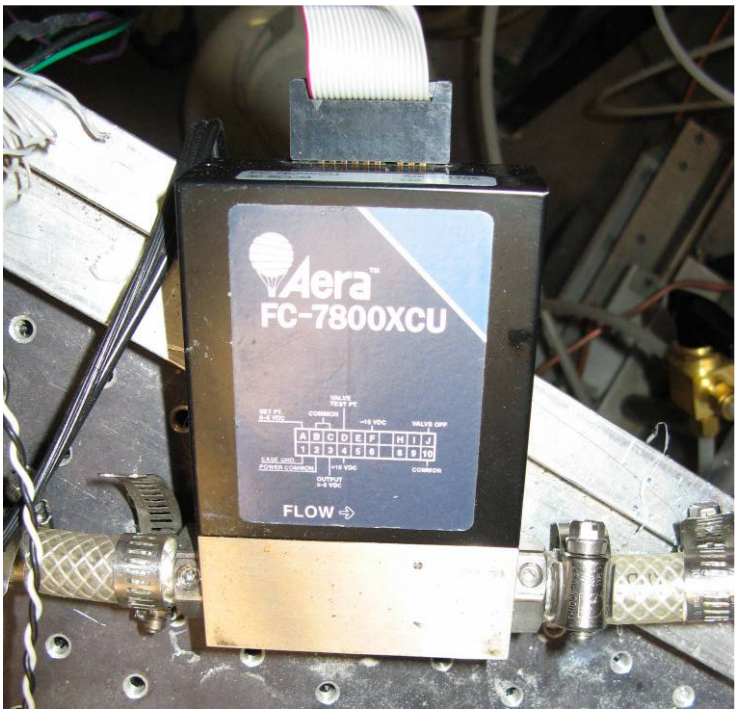

Figure 2.1: Photograph of electronic flow controller used in tube furnace system.

The rotameters were mounted to a flow manifold system shown in Figure 2.2. The outlet of the electronic flow controller was also connected to the manifold, which mixed all the gases and directed them into the tube. For growths in the tube furnaces, quartz tubes were used to contain the source materials and the growth samples. A quartz tube (22 mm inside diameter by 25 mm outside diameter by 5 feet in length) was used because the strain temperature of quartz is 1120ºC (Technical Glass Products 2009), which is higher than all of the experiment temperatures. A 3 foot long nylon bristle brush was used to remove powder that condensed in the tube after each growth.

Figure 2.2: Photograph of flow control manifold used in tube furnace system.

The rotameters were calibrated using air with two different volume measurement devices and a stop watch. The first volume measurement device used was a piston and cylinder volume meter which had a leak rate of 23 mL/min and a resolution of 250 mL. This device was used to calibrate rotameter 18 and rotameter 98. The other volume measurement device was an inverted graduated cylinder in a bucket of water with a resolution of 12.5 mL. The inverted graduated cylinder was initially filled with water, and the flow from the rotameter being calibrated filled the cylinder with air, displacing the water. The graduated cylinder device had no leak so it was used for calibrating

rotameter 90 as it had a much smaller flow rate than the other two rotameters. The results of these calibrations are plotted in Figure B.1, Figure B.2, and Figure B.3.

A combination of copper, stainless steel, and Teflon tubing was used to connect the flow from the rotameters to the quartz tube. Swagelok tube to Cajon O-ring fittings were used to connect the Teflon tubing to the quartz tube which was mounted in two tube furnaces. These fittings are shown in Figure 2.3.

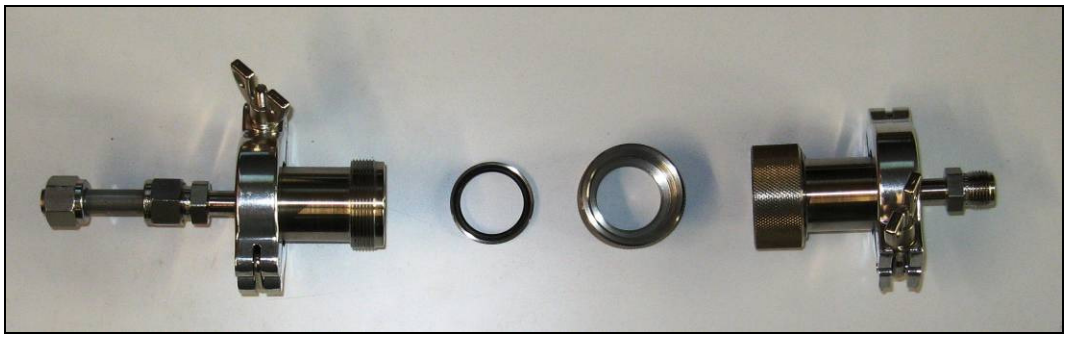

Figure 2.3: Swagelok compression to O-ring fittings used in tube furnace system. (Rostedt 2009)

A photo of the tube furnaces is shown in Figure 2.4.

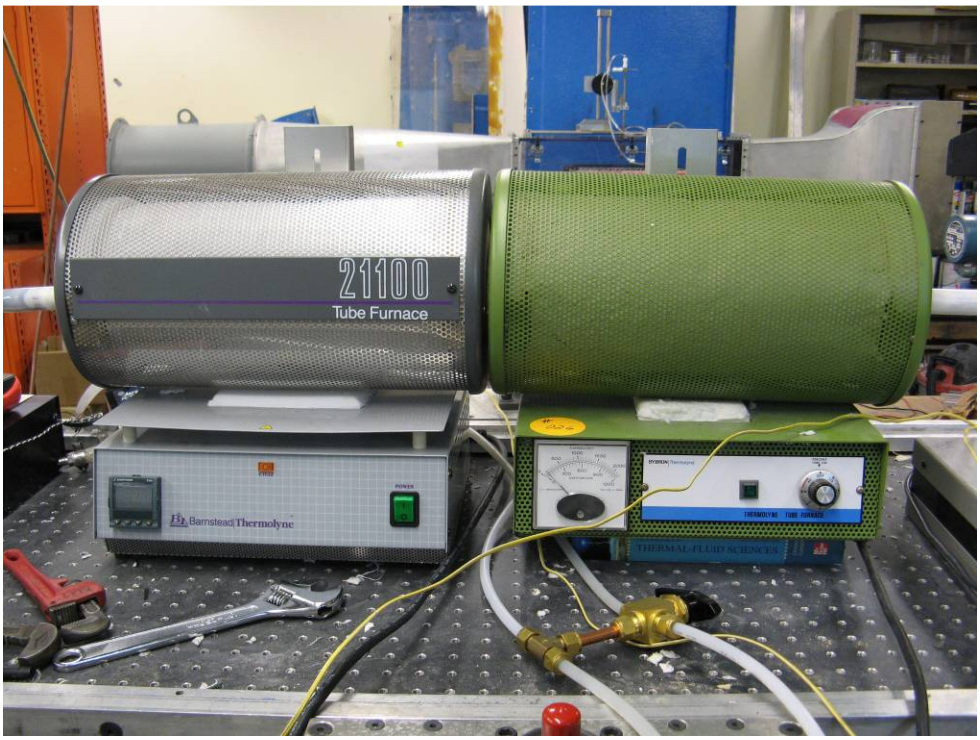

Figure 2.4: Photograph of tube furnace growth setup. The green furnace is upstream.

In Figure 2.4, the green tube furnace on the right was upstream with respect to the gas flow, and the grey furnace on the left was downstream. The upstream furnace was a Barnstead Thermolyne model 21100, and the downstream furnace was a Thermolyne model F-21115. The green tube furnace had a duty cycle control knob with no feedback control, and plot of steady state temperature versus control knob setting is shown in Figure B.4. The thermocouple used to measure furnace temperature was inserted in the middle of the upstream furnace inside the quartz tube. The downstream furnace had a temperature controller so there was no need to plot steady state temperature as a function of control setting, but a plot of spatial temperature variation as a function of set point temperature will be presented in Figure C.2. The thermocouple for the downstream furnace was located in the center of the furnace just outside the of the quartz tube.

The source vapors were produced from powders in a 3 inch long quartz boat in either the upstream furnace or the downstream furnace. The boats that contained ZnO and graphite powder are shown in Figure 2.5. Either of the two boats was used during each experiment.

Figure 2.5: Photograph of boats that contained source powders used in both furnace systems.

For experiments that used an oxidizing gas flow, a Swagelok T-fitting was used just downstream of the tube to Cajon O-ring fitting so that a 1/16" stainless steel tube could be inserted into the furnace. This stainless steel tube injected oxidizer flow about 10" inside from the downstream end of the downstream furnace, just upstream of the middle of the furnace. A schematic of this setup is shown in Figure 2.6.

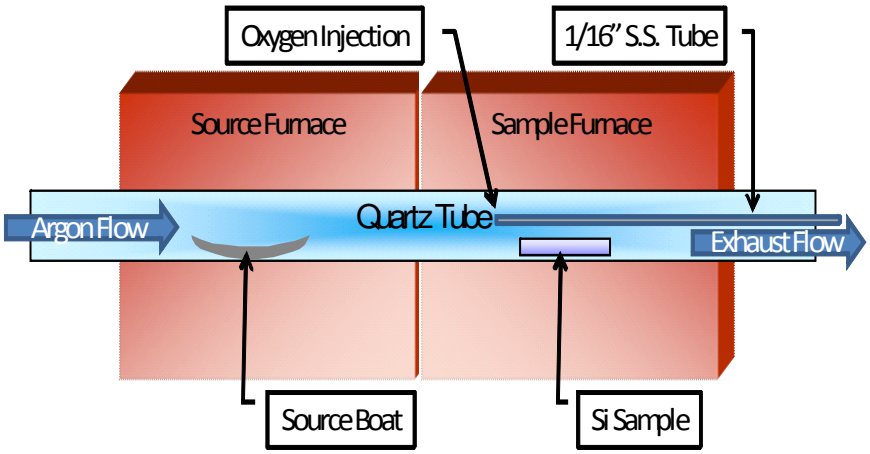

Figure 2.6: Schematic of tube furnace system oxygen injection setup. Dilute O_2 is flowed through the grey S.S. tube and mixes with Ar at the site labeled "Oxygen Injection."

After flowing through the tube furnaces and through the downstream tube to Cajon O-ring fitting, the vapors were passed through a bubbler shown in Figure 2.7.

Figure 2.7: Waste gas bubbler used in tube furnace system. (Rostedt 2009)

The purpose of the bubbler was to capture solid particles that condensed out of the gas flow by dissolving them in water. After passing through the bubbler, the gases flowed to a fume hood. A schematic of the entire tube furnace growth system is shown in Figure 2.8. The purpose of this schematic is to show the flow path of the gases used in the experiments.

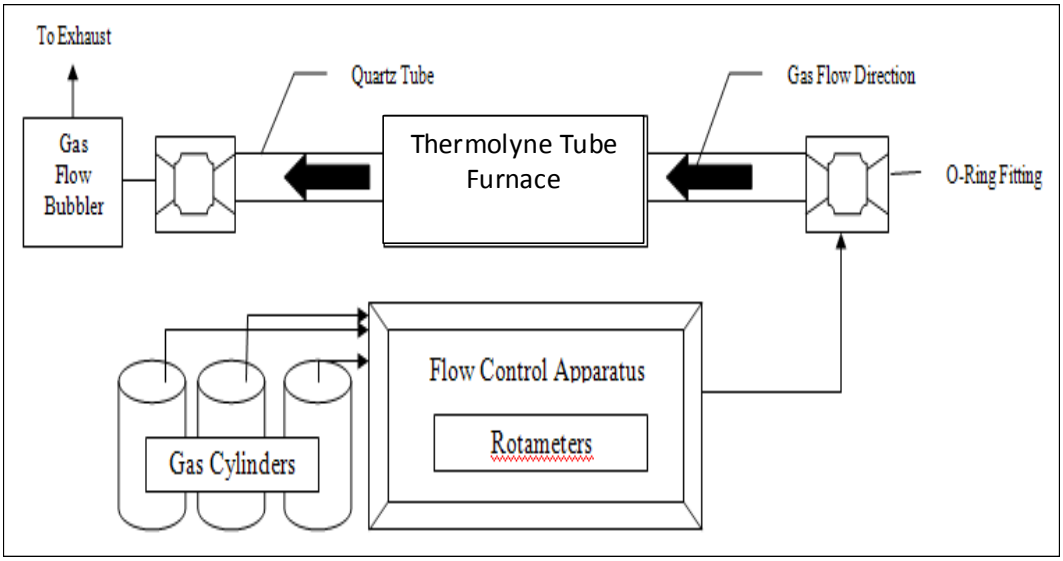

Figure 2.8: Schematic of tube furnace growth system. (Rostedt 2009)

2.3 BENCH-TOP FURNACE

2.3.1 Bench-top Furnace Description

More recent nanowire growth experiments have been carried out in a Jelrus Temp-Master MA bench-top furnace shown in Figure 2.9.

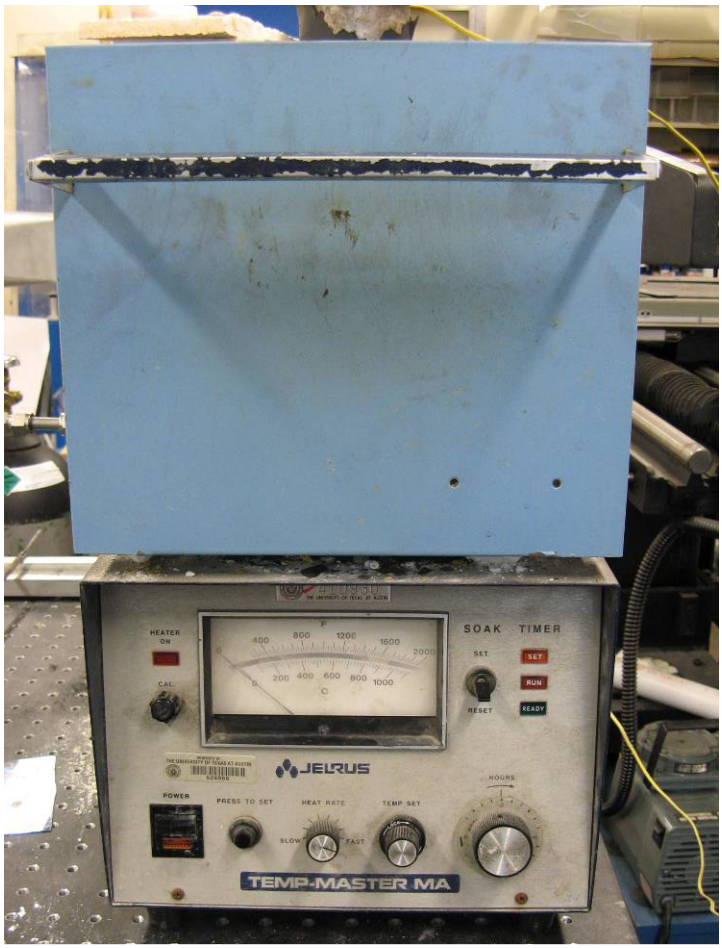

Figure 2.9: Photograph of bench-top furnace.

This furnace had a maximum temperature of 1100ºC and is approximately 6 inches wide by 6 inches deep by 5 inches high. This setup was less complicated than the tube furnace system, and no gas flows were used. In order to reduce temperature fluctuations when inserting and removing samples, a large 0.5” x 5” x 5” stainless steel slab was inserted in the bottom of the furnace. This increased the time needed for the furnace to reach steady state, but it greatly reduced the time between runs and the time to reach steady state after opening the door to insert a sample.

2.3.2 Bench-top Furnace Sample and Source Holder Descriptions

The first sample holder used was a quartz Petri dish with a quartz plate for a lid. The quartz plate lid was used in all experiments with the quartz Petri dish. Pyrex could not be used because the growth temperatures were higher than the melting point of Pyrex. This was determined empirically.

More recently, a stainless steel chamber was fabricated to take advantage of a potentially significant buoyancy effect of the vapors produced by the source powders. A photo of the chamber is shown in Figure 2.10.

Figure 2.10: Photograph of stainless steel chamber. The square plate in the foreground was used to close the open end, and the hose clamp was used to hold the square plate in place. The other end was sealed with a square piece of alumina insulation and ceramic cement.

The chamber was made from a 1 inch rectangular 316 stainless steel tube with 0.065 inch wall thickness. First, a ¼ inch slot was machined in a 6 inch long segment of tube. Then, another 6 inch long segment of tube was cut to ¼ inch in height and welded onto the

bottom of the first segment so that the slot was facing the new segment. This formed a top chamber that was approximately 1 inch wide by 1 inch high by 6 inches long and a bottom chamber that was approximately 1 inch wide by 0.185 inches high by 6 inches long. The top chamber contained the same source boat used in the tube furnace, and it was sealed with a piece of alumina insulation and ceramic cement on one end. On the other end, a stainless steel plate covered the opening, and a hose clamp held this plate in place. The bottom chamber was open at both ends, and the sample was placed face up in this chamber so that diffusion flow would flow through the slot, impinge on the sample, and then flow across the sample. A schematic illustrating the flows of vapor species is shown in Figure 2.11.

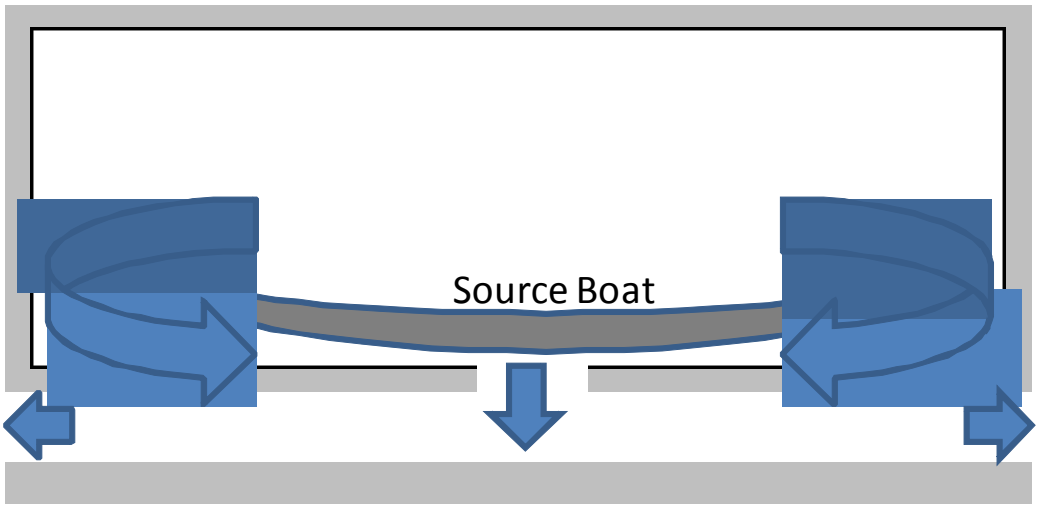

Figure 2.11: Conceptual schematic of how the stainless steel growth chamber was expected to work. Arrows represent gas diffusion flow.

The source boats seen in Figure 2.5 were also used in the bench-top furnace experiments in conjunction with both the quartz Petri dish and the stainless steel chamber.

The most recent sample holders were fabricated from quartz boats in order to hold the samples on a pair of beams suspended less than 1 mm above a powder surface and are shown in Figure 2.12.

`

Figure 2.12: Photograph of quartz boats for bench-top furnace nanowire growth.

2.4 CHARACTERIZATION

Nanowires were characterized using a Canon PowerShot A710 IS digital camera and a Supra Variable Pressure SEM. The camera was used for taking macroscopic photographs of samples, and the SEM was used for obtaining images of nanowires.

Chapter 3: Experimental Procedures

3.1 Powder and Sample Preparation

3.1.1 Powder Weighing and Grinding

Powder was massed using the triple beam balance. The ZnO and graphite powder were always mixed in an equimolar ratio, which is 6.78 grams of ZnO for each gram of graphite. A plastic jar was placed on the balance, and then the balance was tared. Next, an arbitrary mass of graphite was added to the jar, and the weight was noted. This number was multiplied by the molecular weight ratio to determine the new target mass. ZnO powder was added until this mass was achieved; an overshoot of up to 10 grams was considered acceptable. Because the ratio of ZnO to C was more sensitive to the mass of C, the ZnO was weighed second.

After capping the jar and thoroughly shaking the powder mixture, about 12 cm^3 was poured into the mortar and ground up with the mortar and pestle. The grinding was performed on a growth by growth basis because the powder mixture was uniform on a large scale, but there were small chunks on the order of 3 mm in diameter of mostly ZnO that needed to be broken up to ensure uniform mixture for the amount of powder needed for one growth. The grinding also ensured a more intimate contact between graphite and ZnO powder, which should increase the vapor production rate. It should be noted that this grinding step was not added until later experiments. The effects of this will be discussed in the next chapter.

3.1.2 Dicing Saw and Sample Preparation

For wafer fabrication, a dicing saw was used to ensure uniform sample size. One 150 mm wafer could be cut into 6 76.2 mm by 20 mm samples. Each cut distance was

increased by 200 μm from the desired sample dimension to account for dicing saw blade kerf.

The dicing saw used water to cool the blade, and this produced a slurry of Si dust. After dicing the wafers, to remove this Si dust slurry, the samples were rinsed in deionized water and blown dry with pure N_2 gas. Since the wafer containers were never opened outside of a clean room, this should have resulted in a reasonably clean surface. In earlier experiments, the wafers were also sonicated in isopropanol, ethanol, and deionized water, but this step was later omitted because it did not seem to affect the experimental results.

3.1.3 Catalyst Deposition

For early experiments, a thermal evaporator with a quartz crystal deposition monitor was used to deposit the thin film catalyst. None of the data from these experiments will be presented in this thesis. Growth methods were improved and refined since the use of thermal evaporation was ceased, but thermal evaporation could likely be used with more recent growth parameters without impacting these results.

More recently, and currently, sputter coating was the preferred method for applying the catalyst layer to the samples. Sputter coating takes less time and is less expensive for a large number of experiments. When using the sputter coater, 2 samples were placed in a Petri dish which was set in the coater. This prevented the samples from being dropped into the sputter coater and/or being broken.

3.2 TUBE FURNACE

3.2.4 Tube Furnace Growth Parameters

The parameters that were varied in the tube furnace experiments were metal layer thickness, downstream furnace set point temperature, upstream furnace setting, number

of furnaces used, annealing time, growth duration, primary atmosphere gas species, flow control device(s), oxidizer flow rate, O_2 concentration of oxidizer, location of sample, and location of source. Annealing time is the amount of time the sample was exposed to the growth temperature without being exposed to the source vapors. Annealing was sometimes used in order to ensure that the Ostwald ripening process that formed the Au nanoparticles was complete when the growth was started. As sputter coating applies Au particles, and not a thin film, annealing was not expected to be necessary.

The growth parameters in the first experiment on January 26, 2009 were intended to test the effect of a large range of temperature on the nanowire growth. The sample was protruding 3/8 inch out of the downstream end of the downstream furnace, and the source boat was immediately upstream of the sample. The upstream furnace was not used for this experiment. Argon was flowed at 25 sccm using the electronic flow controller. The high temperature gradient near the downstream end of the furnace exposed the sample to a temperature range from just above room temperature to the set point temperature of 900ºC. The next three experiments had the same growth parameters except for duration which was varied from 1 to 20 minutes. We hoped to see how the growth progressed with time.

Starting with the February 4, 2009 experiment, the experiments through February 12 tested the effects of metal layer thickness by varying metal layer thickness from 2 nm to over 50 nm. The flow rate was set to 50 mL/min using to the plastic bead of rotameter 18 for the first 7 of these experiments, and it was not varied by more than an order of magnitude over the entire set. The sample was centered in the downstream furnace at a temperature set point of 900ºC, and the source boat was centered in the upstream furnace at a temperature setting of 5.

Experiments from February 17, 2009 until March 11 tested the effect of oxygen injection through the 1/16 inch nominal diameter stainless steel tube. O_2 concentration was changed from 21% to 5%, but this was not the only variable. Ar flow rate was varied from 24 mL/min to 64 mL/min, temperature was varied from 800ºC to 912ºC. In all but one case, the sample was centered in the downstream furnace and the source boat was centered in the upstream furnace. The exception was with the boat immediately upstream of the sample which was centered in the downstream furnace.

Starting with the growth on March 13, 2009, the only parameters that were varied were location of sample and location of source boat. Variations were as follows: sample face down on top of source boat in the middle of the downstream furnace, sample face up on top of source boat in the middle of the downstream furnace, and source powder directly on sample in the middle of the downstream furnace.

On April 2, 2009, two previous growth conditions were repeated with CO_2 instead of Ar. One of these was with the sample centered in the downstream furnace with the source boat immediately upstream and the other was with the sample face down on top of the source boat.

The remaining growths tested the effect of a high flow rate and variation in location of the sample. The flow rate was set to 3300 mL/min using rotameter 98, and the source boat was placed 84 cm into the tube in the upstream furnace. The samples were placed anywhere from immediately downstream of the source boat to the center of the downstream furnace.

A comprehensive set of all tube furnace growth parameters is shown in Table A.1.

3.2.5 Tube Furnace Experimental Procedure

Cleaning the quartz tube was necessary to remove powders that condense during growths and as the tube cools after growths. Throughout the research, the tube was brushed with the bristle brush whenever large amounts of powder collected in the bottom of the tube. We made the assumption that it was unnecessary to clean the tube more thoroughly, as in an acid bath, since contamination would probably have a similar effect from one experiment to the next. Also, cleaning in an acid bath required the tube to be taken to an off campus facility so it was inconvenient. High temperature air flows were also sometimes used to oxidize carbon deposits on an as needed basis.

The procedure for inserting and removing the sample and source boat was changed several times since the first experiments. Initially, only one furnace was used, and after reaching steady state growth temperature, the source boat was inserted in the quartz tube from the downstream end and allowed to rest on the bottom of the tube. After 5 to 10 minutes of Ar flow to purge the tube of O_2, the sample was placed in the quartz tube from the downstream end and due to its width, rested in the middle of the tube. At the end of the growth, the furnace was turned off and allowed to cool to room temperature. When the furnace returned to room temperature, the sample and source boat were removed. This procedure was used on January 26, January 27, and the first two runs of January 28.

In the next iteration, both furnaces were used. When the furnaces had reached steady state, the sample was inserted from the downstream end. Then, Ar was flowed at a high enough rate to cause violent bubbling in the bubbler; this resulted in a flow outside the range of the rotameter. After 5 to 10 minutes of this, the source boat was inserted from the upstream end. Then the Ar flow rate was set to the growth flow rate using rotameter 18. After the growth was complete, the source boat was removed and the

upstream furnace was turned off. Air was then flowed through the quartz tube for 10 minutes to oxidize any carbon powder in the tube or on the sample. Lastly, the downstream furnace was turned off, and the sample was removed. This procedure was used in the last run of January 28, the 3rd and 4th runs of February 11, and the 2nd run of February 12.

The next growth procedure was to insert the source boat and sample from the downstream end of the tube with Ar flowing. This reduced the amount of O_2 being allowed into the tube and eliminate the need for Ar purging. After growth was complete, the samples were removed, and either the furnace was turned off or another growth was started. This procedure was used for the first two runs of February 11.

In the next revision, the source and sample were inserted into cold furnaces with Ar flowing at the growth flow rate. The downstream furnace was brought to the annealing temperature, and after annealing, the upstream furnace was turned on. When the upstream furnace reached steady state, the growth time was officially started. At the end of the growth, both the sample and source boat were removed. This procedure was used on February 12 only.

The final procedure was followed consistently from March 13, 2009 onward. When both furnaces reached steady state with Ar flowing at the growth flow rate, the sample was inserted in the downstream furnace. After annealing, if the sample was annealed at all, the source boat was inserted from the upstream end and the growth time was officially started. If oxidizer injection was used, the flow of air or dilute O_2 was started at this time. When the growth was finished, the sample and source were removed, and either another growth was started or the furnaces were turned off.

3.3 BENCH-TOP FURNACE

3.3.6 Bench-top Furnace Growth Parameters

Bench-top furnace growth parameters were catalyst thickness, catalyst material, furnace temperature, growth duration, type of container used, location of source powder, and location of sample. All samples were sputter coated.

The first growth on April 22 was in the quartz Petri dish. This Petri dish was used for all four growths in April, and it was also used on May 29. All of these growths were testing for effects caused by changing the locations of the sample and the source. During the first growth, the sample was face up in the center of the Petri dish in between two of the source boats that were used in the tube furnace experiments. This was changed to loose powder surrounding the sample in the bottom of the Petri dish during the next growth. The two growths on April 23 both had the sample face down about 1 mm above the loose powder supported by two stacked 20 mm by 10 mm pieces of Si wafer on either end. The final growth with this setup on May 29 was a repeat of the experiment with the sample face up in the center of the Petri dish surrounded by loose powder.

The growths from May 26 through June 3 were done in the stainless steel growth chamber. For the first three of these, the source boat was placed in the top portion of the chamber which was sealed by the hose clamp and stainless steel plate. The sample was face up in the bottom portion of the chamber. For the third of these growths, growth duration was increased from 1 hour to 5 hours.

The first growth on May 29 was slightly different because the sample was placed on top of the source boat in the top portion of the stainless steel chamber. During this growth, the hose clamp was improperly tightened so the end-cap that normally sealed the stainless steel chamber fell off, allowing more than usual exposure of the sample and source powder to air. This was repeated in two growths on May 29. On June 1 and June

2, the only change was that a 5 inch long source boat was used instead of the 3 inch source boat. Two growths on June 5 were repeats of the growth with the long boat, but the shape of the powder surface was changed from being flat to convex upward.

Starting on June 11, all of the remaining growths were done in the boat with beams shown in Figure 2.12. The degree of concavity or convexity of the powder surface, along with the growth time and the type of catalyst, were varied. The most important of these variables was powder surface profile.

A comprehensive set of all growth parameters used for the bench-top furnace are shown in Table A.1 and

Run	Date	Catalyst Thickness (nm)	Catalyst Metal	Deposition Technique	Furnace Setpoint (°C)	Growth Duration (min)	Location of Sample	Location of Source
1	4/22/09	2.5	Au	Sputter*	920	30	center of petri dish	2 boats on either side of sample
2	4/22/09	2.5	Au	Sputter*	1000	30	center of petri dish	loose powder surrounding sample
1	4/23/09	2.5	Au	Sputter*	1000	30	face down ~1 mm above powder on Si supports	uniform layer in petri dish
2	4/23/09	2.5	Au	Sputter*	1000	30	face down center of petri dish	~1 mm underneath sample
1	5/26/09	2.5	Au	Sputter*	1000	60	bottom chamber of SS tube	top chamber of SS tube reactor
1	5/28/09	2.5	Au	Sputter*	1000	60		

2	5/28/09	2.5	Au	Sputter*	1000	300	reactor	
1	5/29/09	2.5	Au	Sputter*	1000	60	top chamber of SS tube reactor face down on source boat	short boat in open top chamber of SS tube reactor beneath sample
2	5/29/09	2.5	Au	Sputter*	1000	10	center of petri dish	loose powder surrounding sample
1	6/1/09	2.5	Au	Sputter*	1000	60	top chamber of SS tube reactor face down on source boat	long boat in top chamber of SS tube reactor beneath sample
2	6/2/09	2.5	Au	Sputter*	1000	10		
1	6/3/09	2.5	Au	Sputter*	1000	60	face down in 5" long 22mm quartz tube	~1 mm underneath sample
1	6/5/09	2.5	Au	Sputter*	1000	10	top chamber of SS tube reactor face down on source boat	long boat in top chamber of SS tube reactor beneath sample. Flat powder surface.

2	6/5/09	2.5	Au	Sputter*	1000	10		long boat in top chamber of SS tube reactor beneath sample. Powder surface convex up.
1	6/11/09	2.5	Au	Sputter*	1000	30	face down on beams of boat	below beams of ~25 mm wide boat
2	6/12/09	0.0	Au	n/a	1000	15	face down on beams of boat	below beams of ~25 mm wide boat
1	6/17/09	2.5	Au	Sputter*	1000	60	face down on beams of boat	below beams of ~25 mm wide boat
1	6/22/09	2.5	Au	Sputter*	1000	10	face down on beams of boat	packed down with wafer and scraped to be even with beams
1	7/3/09	2.5	Au	Sputter*	1000	15	face down on beams of boat	scraped to have small concavity
2	7/3/09	2.5	Au	Sputter*	1000	15	face down on beams of boat	scraped to have large convexity
3	7/3/09	2.5	Au	Sputter*	1000	15	face down	scraped to have large

							on beams of boat	concavity
4	7/3/09	2.5	Au	Sputter*	1000	17	face down on beams of boat	packed and scraped to have large concavity, covering gap on side of sample
5	7/3/09	2.5	Cu	Sputter*	1000	15	face down on beams of boat	

Table A.2.

3.3.7 Bench-top Furnace Experimental Procedure

The bench-top furnace procedure was simpler than the tube furnace system. The furnace was turned on and allowed to reach steady state temperature. The freshly ground ZnO and graphite powder were placed in the growth vessel, and the sample was placed near the powder.

Specifically for the boats in Figure 2.12, powder would be dumped into the boat then packed down with a scrap Si sample. Powder would be scraped out to control the vertical distance between the powder and the sample and to modify the contour of the powder surface. The packing of the powder was done to ensure that any chunks that remained after using the mortar and pestle were packed down. Typically, to control whether the powder surface was concave or convex in the upward direction, a piece of brass shim of the same width as the boat would be cut to have the desired profile. Then, it would be used to scrape the powder away to have either an upwardly convex or concave surface. After preparing the powder surface, the last step was to place a Si sample face down on the beams of the boat, just above the powder. In the last two experiments of July 3, 2009, we piled additional ZnO and graphite powder over a small

gap between the edge of the Si sample and the side of the boat. This was intended to block air from diffusing into the small volume between the sample and the powder.

For the growths in the Petri dish, powder was poured either in the Petri dish or the source boats, and the sample was placed according to the growth parameters for each experiment.

For growths in the stainless steel chamber, the source boat was filled with powder and placed in the top portion of the chamber. As already noted in the previous section on growth parameters, the sample was placed either in the bottom portion of the chamber face up or face down on the source boat in the top portion of the chamber.

Chapter 4: Results and Discussion

The purpose of this chapter is to show the results of the growth methods and to discuss these results. The goal was to achieve an improved understanding of the growth processes and/or growth parameters that resulted in successful growth. Two metrics were used to characterize the success of nanowire growth, both of which are somewhat qualitative.

The first metric is coverage of the sample. This is a quantitative metric and will be expressed as percent coverage. Alternatively, a verbal description is sometimes provided. Percent coverage is determined visually based on the presence of a white powdery film that can be seen wherever nanowires are present. The qualitative aspects are presented in the form of photographs of samples. All photos are magnified by approximately 50% from actual size. Photos are presented with relevant growth conditions.

The second metric is morphology of nanostructure. The SEM was used to determine nanowire length, diameter, and shape. In addition to nanowires, microwires, nanocombs, nanoribbons, and other nanostructures were grown. Microwires are nanowires with diameters greater than 1 μm, nanoribbons are two dimensional nanostructures less than 1 μm thick, and nanocombs are a combination of nanoribbons and an array of parallel nanowires. Morphology refers to these types of descriptors.

For reference, a photograph of a bare Si sample is shown in Figure 4.1. Note that this sample is highly reflective.

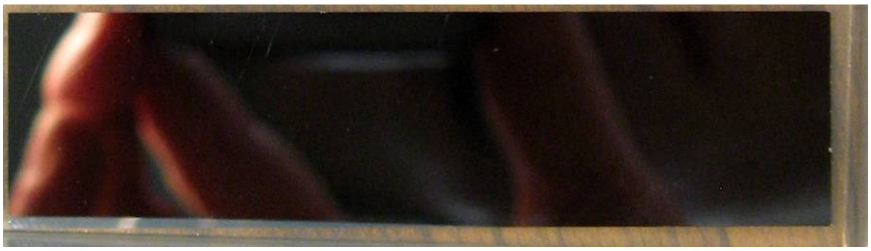

Figure 4.1: Photograph of bare Si sample.

An SEM image of a sample with only the Au coating is shown in Figure 4.2.

Figure 4.2: SEM image of sample sputter coated with 1 nm of Au. The upper left corner was shadowed during the coating, leaving a bare Si surface.

Note that the only objects seen on the surface of the sample are Au nanoparticles that are typically about 10 nm in diameter. The area in the top left corner is a bare Si surface. Note the lack of texture in this uncoated area. With this reference in mind, nanowire growth results are presented next. Growths which produced no visible change in sample appearance are not presented.

For a complete listing of all growth conditions, see Table A.1 and Table A.2.

4.1 TUBE FURNACE

Our initial attempts at ZnO nanowire growth were done using a tube furnace, replicating the methods we found in the literature that other researchers had success with.

4.1.1 Tube Furnace Growth Procedure Evolution

Initially, we tried to duplicate the experimental procedures of Yang, et al. (2002). We used thermal evaporation to coat several 0.5 cm x 0.5 cm <100> Si wafers with 10 nm of Au. We then placed these samples 1cm to 10 cm downstream from a source boat which was filled with ZnO and C powder in equal amounts by mass. We used Ar flow rates of 25 sccm, growth temperatures from 850ºC to 1000ºC, and annealing of up to 30 minutes at the growth temperature. This procedure sometimes produced small patches of nanowires, but there was no reproducibility. At best, the samples were less than 10% covered with nanowires.

The boiling temperature of Zn is 907ºC (American Elements 2009), and we thought this might be a critical temperature. We thought that maintaining the sample at a temperature low enough that Zn condensation would occur might result in dense growth. In order to test this hypothesis, the two tube furnace system was implemented. This enabled us to use different controlled temperatures for the souce boat and the sample so that the source boat could be at a high enough temperature for carbothermal reduction and the sample could be below the boiling temperature of Zn. In these experiments, the source boat was in the middle of the upstream furnace, 15 inches upstream of the single 20 mm x 76.2 mm sample in the middle of the downstream furnace. The sample was annealed at the growth temperature in some of these experiments, and the Ar flow rate was 24 sccm. The samples were sputter coated with 2.5 nm Au. We used a 1:1 molar

ratio of ZnO:C from this point forward after noticing that several groups specified a 1:1 ratio on a molar basis rather than a mass basis. Using a source furnace temperature of approximately 1000ºC and a sample furnace set point temperature of 800ºC, we achieved one growth with greater than 50% coverage, but we were never able to repeat this success. In addition, sample furnace temperatures lower than 900ºC often resulted in formation of Zn balls as large as 2 mm in diameter caused by Zn condensation. An SEM image of a Zn ball produced by condensation at a temperature below 900ºC is shown in Figure 4.3.

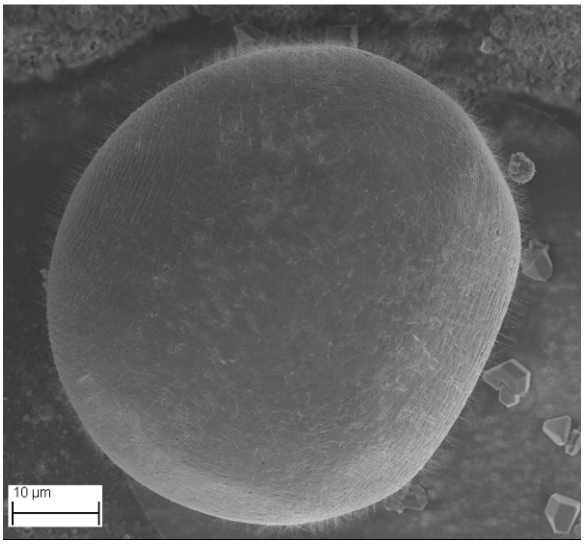

Figure 4.3: SEM image of Zn ball grown with sample furnace at 800ºC. Nanowires are visible on surface of Zn ball. The ball was around 100 µm in diameter and was visible to the naked eye.

This ball is a typical result for growths with the sample furnace set below 900ºC. Many samples were covered with Zn balls of this size and larger. The results were inconsistent with nanowires being produced in only some of the experiments, and overgrowth caused by self-catalysis occurred. This undesirable overgrowth was the formation of 3-dimensional structures with a low surface area. These 3-dimensional structures were typically faceted, low aspect ratio,

and about 1 μm^3 in volume. This is likely due to the VLS catalytic mechanism being overwhelmed by Zn condensation. Nanowires were rarely grown anywhere other than the surfaces of the balls.

Lack of success with independently regulating the source boat and sample furnace temperatures led us to test the effect of flowing dilute O_2 through the quartz tube. We thought O_2 might oxidize Zn more readily than CO. It was found that exposing the source powder to an oxidizing atmosphere caused oxidation of graphite to compete with the carbothermal reaction for graphite. This nearly eliminated production of Zn vapor and did not produce nanowires. To remedy this problem, we began using the oxygen injection rig shown schematically in Figure 2.6 which introduced O_2 downstream of the source boat. Ar/N_2 gas with 5% O_2 or air with 21% O_2 was flowed at 6 sccm against an Ar flow ranging from 24 sccm to 64 sccm. The sample and source boat were centered in the downstream and upstream furnaces, respectively. Large microwires on the order of 1 cm in length by 100 μm in diameter were found in the quartz tube near the O_2 injection site. The reaction zone where ZnO was produced was located at the interface between the Zn vapor and O_2 concentration flows. In a manner analogous to a diffusion flame, the location of the the reaction front was tunable based on relative flow rates of Ar and oxidizer injection. Increasing the Ar flow rate would carry the source vapors farther downstream in the tube before they were fully oxidized, shifting the location of the ZnO-producing reaction front downstream. By tuning this reaction front to occur at the location of the sample, ZnO powder was made to condense on the sample. An SEM image of this powder is shown in Figure 4.4.

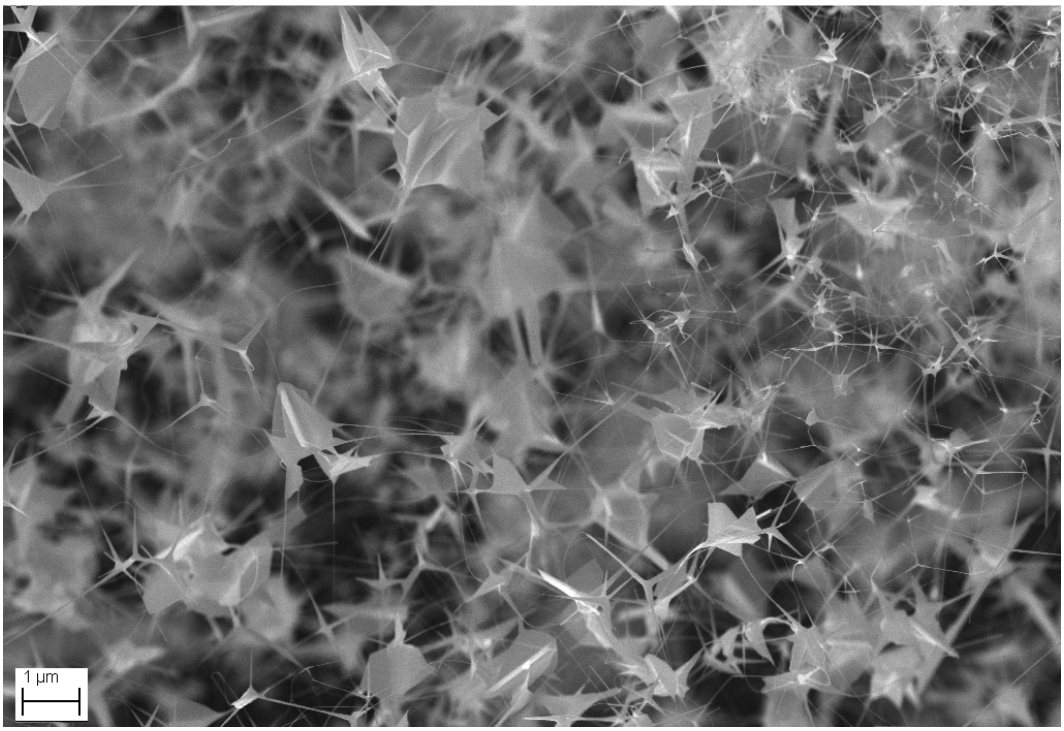

Figure 4.4: SEM image of ZnO powder that condensed from the vapor phase. This occurred if O_2 was injected because Zn vapor reacted with O_2 to produce vapor phase ZnO. Nanowires are visible, but the powdery material in this photo was loosely fixed to the surface.

The nanowires shown in Figure 4.4 were relatively long (~1µm) and had a high aspect ratio, but the growth was only loosely attached to the surface. By blowing on these samples with breath alone, the powder and nanowires could easily be removed. The O_2 injection experiments, while they did produce large quantities of nanowires, did not result in a durable substrate for catalysis.

After many unsuccessful experiments with two tube furnaces, we tried to determine the cause of the problem. Through changing temperature conditions we found the problem was not the operating temperatures. We then began to consider that the gas-phase concentrations of Zn vapor and oxidizer were not optimal. One possibility was that the high molecular weight Zn/CO/CO_2 vapor was flowing below our wafer or not mixing with the oxidizing gas or that the Zn vapor and oxidizer were reacting upstream of the

sample. We started thinking we should decrease the distance between the source and sample so we decreased this distance from 15 inches to less than an inch. We stopped using the O_2 flow, and Ar was flowed at a higher rate of 3.3 L/min. In some cases, we used one furnace with the sample protruding 3/8" out of the downstream end, and the source was immediately upstream of the sample. The growths from January 26 and January 27, 2009 shown in Figure 4.5 were good examples of results under these conditions. The samples were exposed to a range of temperature from just above ambient up to the growth temperature of 900ºC. In all of the photographs of samples presented in this section the upstream edge is at the left side of the photo.

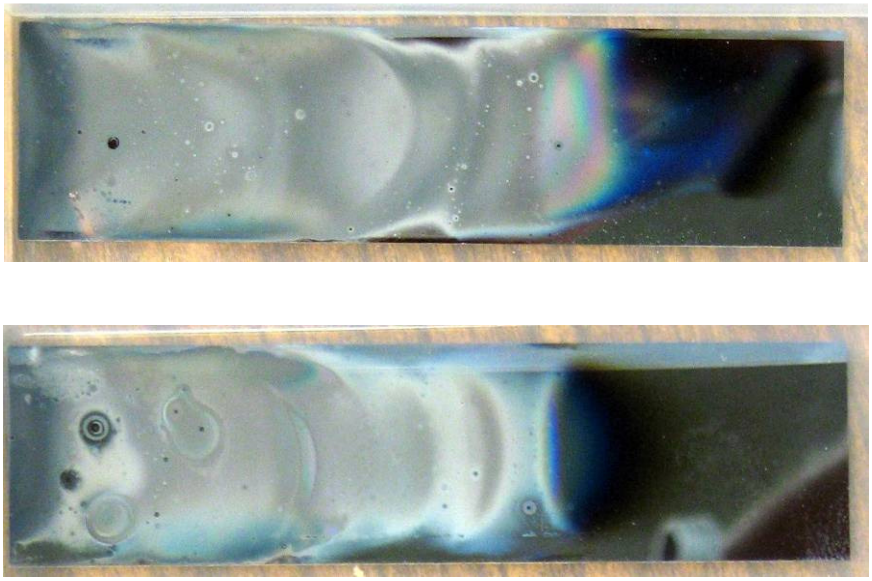

Figure 4.5: Photographs of two tube furnace samples from January 26, 2009 (top) and January 27, 2009 (bottom). The Ar flow rate was 3.3 L/min which was two orders of magnitude higher than previously used. Each sample protruded 3/8" from the furnace and was exposed to a large temperature range. Growth duration was 20 minutes for the top sample and 8 minutes for the bottom sample.

Both growths show parabola shaped depositions which were a consequence of the rapid decrease in temperature with respect to distance along the sample, the difference in

density between Ar and the source vapors, and the high Ar flow rate of 3.3 L/min. The density of nanostructures seemed to decrease with distance from the source boat. This led us to believe that decreasing concentrations of reactant species, caused by mixing with Ar, reduced the flux of Zn atoms to the Au catalyst particles thereby reducing nanowire density. In addition, every experiment thus far had deposited ZnO on the inside of the quartz tube, and we started thinking the inside surface of the tube may have been an additional sink for Zn vapor. The early experiments with the 0.5 cm x 0.5 cm samples may not have produced nanowires as well as the January 26 and January 27 growths because we never tried placing the small samples immediately downstream of the source boat. In the experiments with the large 20 mm x 76.2 mm samples, the vapors from the source boat likely spilled over the walls of the boat and sank down onto the sample which was touching the source boat. If there had been a gap between the source boat and sample, the source vapors would have flowed under the sample due to buoyancy effects. This is probably why the earlier experiments did not result in dense growth.

Shortly after these experiments, we became interested in varying the Au catalyst thickness over several orders of magnitude because this had not yet been attempted. We used both tube furnaces with the upstream furnace maintained at about 950ºC and the downstream furnace set at 900ºC. The samples were sputter coated with 2 nm Au, 10 nm Au, and 50 nm Au. Ar was flowed at 50 sccm. The sample in each experiment was centered in the downstream furnace and the source boat was centered in the upstream furnace. These experiments resulted in some nanowire growth, but the coverage was sparse. Gold thickness did not cause any apparent changes in morphology or sample coverage.

Due to the success observed from decreasing the distance between source boat and sample, we wanted to try experiments with minimum possible distance between the

sample and source boat. The next section will discuss the further evolution of the growth parameters used by presenting photos and SEM images for every growth parameter change discussed.

4.1.2 Repeatable Tube Furnace Results

The first growth, shown in the photo in Figure 4.6 and in the SEM image in Figure 4.7, was done on March 13, 2009. This sample was coated with 2.5 nm Au, the upstream furnace was set to 5, the downstream furnace was set to 900ºC, Ar was flowed at 24 sccm, and the growth duration was 30 minutes. The growth parameter that was unique in this growth was the sample location. This was the first growth in the tube furnace to test the effect of placing the sample face down on top of the source boat. A 5 inch long source boat was used for this growth.

Figure 4.6: Photograph of tube furnace sample from Run 1 on March 13, 2009. The growth parameter being tested was the location of the sample relative to the source. This was the first growth with the sample face down on top of the source boat.

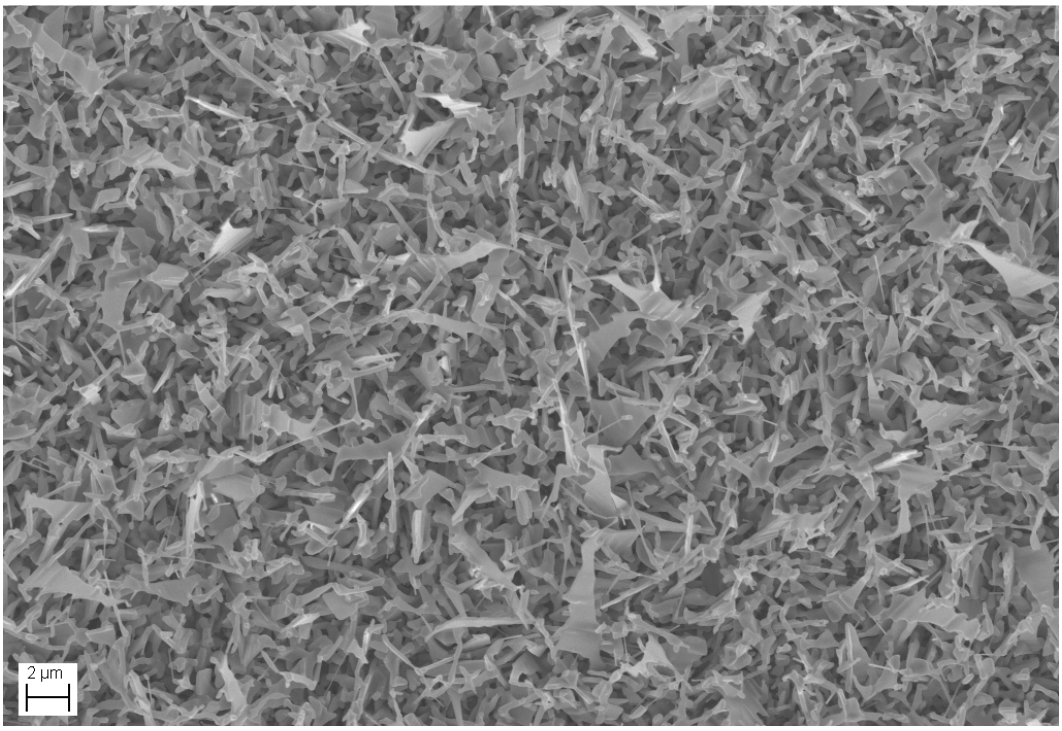

Figure 4.7: SEM image of tube furnace sample from Run 1 on March 13, 2009. The growth parameter being tested was the location of the sample relative to the source. This was the first growth with the sample face down on top of the source boat.

The March 13 growth resulted in less than 10% coverage of the sample, but wherever there was growth, there was high areal nanowire density. The SEM image (Figure 4.7) shows a mix of nanowires and nanoribbons. This magnification of this image is too low to obtain a good estimate of the size of the nanostructures shown. Most, if not all, of the structures in this image were grown by the VS mechanism because no Au tips can be seen. Nanowires are the only structures we grew that can be grown by the VLS mechanism. However, nanowire growth initiated by the VLS mechanism can morph into nanoribbons, microwires, or other structures if the flux of vapor species to the surface becomes high enough to overwhelm the VLS catalyst mechanism.

The next growth, performed on March 18 was a repetition of the March 13 conditions, and the photo and SEM images are shown in Figure 4.8, Figure 4.9, Figure 4.10, and Figure 4.12.

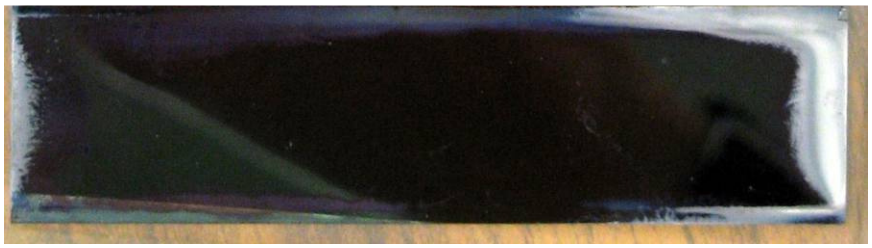

Figure 4.8: Photograph of tube furnace sample from March 18, 2009. The growth parameter being tested was the location of the sample relative to the source. This sample was face down on top of the source boat.

The photo of the sample (Figure 4.8) shows similar results to the March 13 growth, as was expected. There is less than 10% coverage and growth is only on the ends of the sample. Between the March 13 and March 18 growths, there does not seem to be any dependence on which end is upstream. It is likely that reducing the distance between the source powder and the sample was more important than the direction of Ar flow.

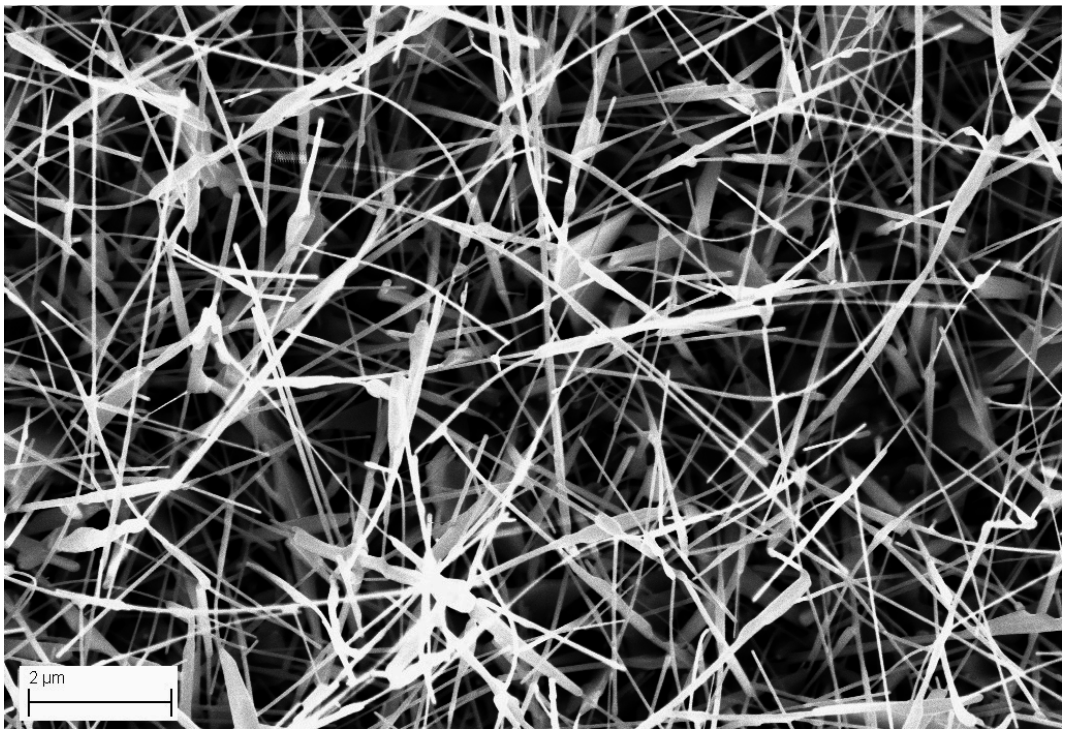

Figure 4.9: SEM image of tube furnace sample from March 18, 2009. The growth parameter being tested was the location of the sample relative to the source. This sample was face down on top of the source boat.

The SEM image in Figure 4.9 shows dense nanowires that are around 5 µm in length and under 200 nm in diameter. No gold tips were found so the VS mechanism was responsible for the growth shown here.

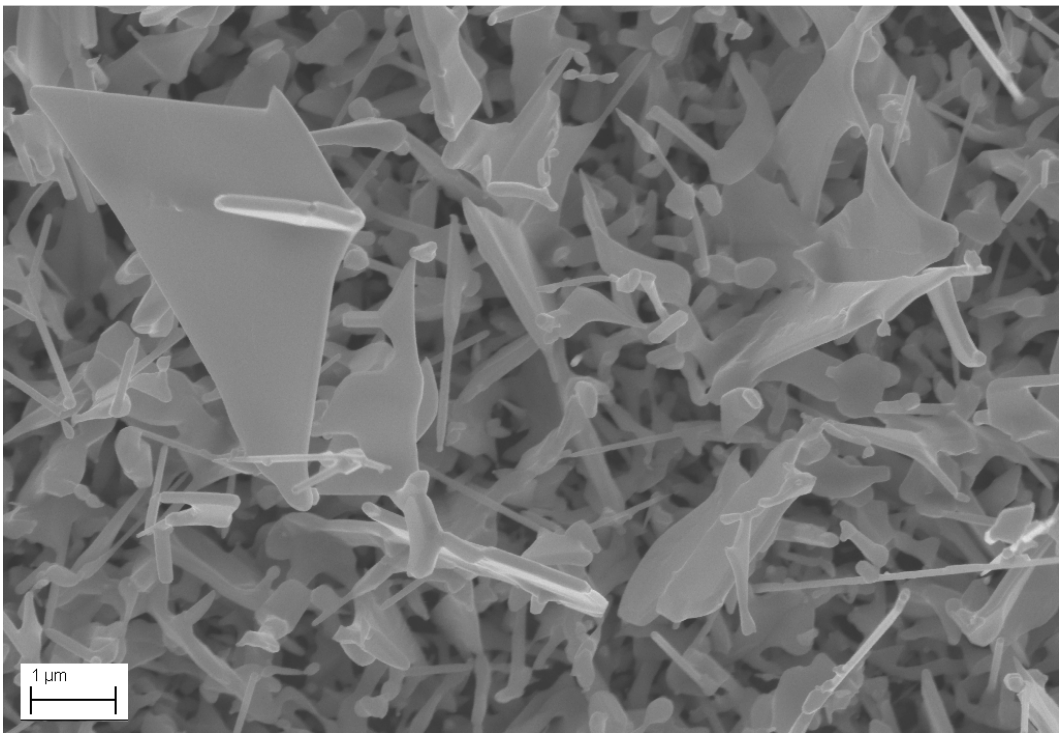

Figure 4.10: SEM image of tube furnace sample from March 18, 2009. The growth parameter being tested was the location of the sample relative to the source. This sample was face down on top of the source boat.

The image in Figure 4.10 shows nanoribbons and other structures formed by the VS mechanism. Most of these structures are microscopic in dimension and only a few nanowires are shown in this image.

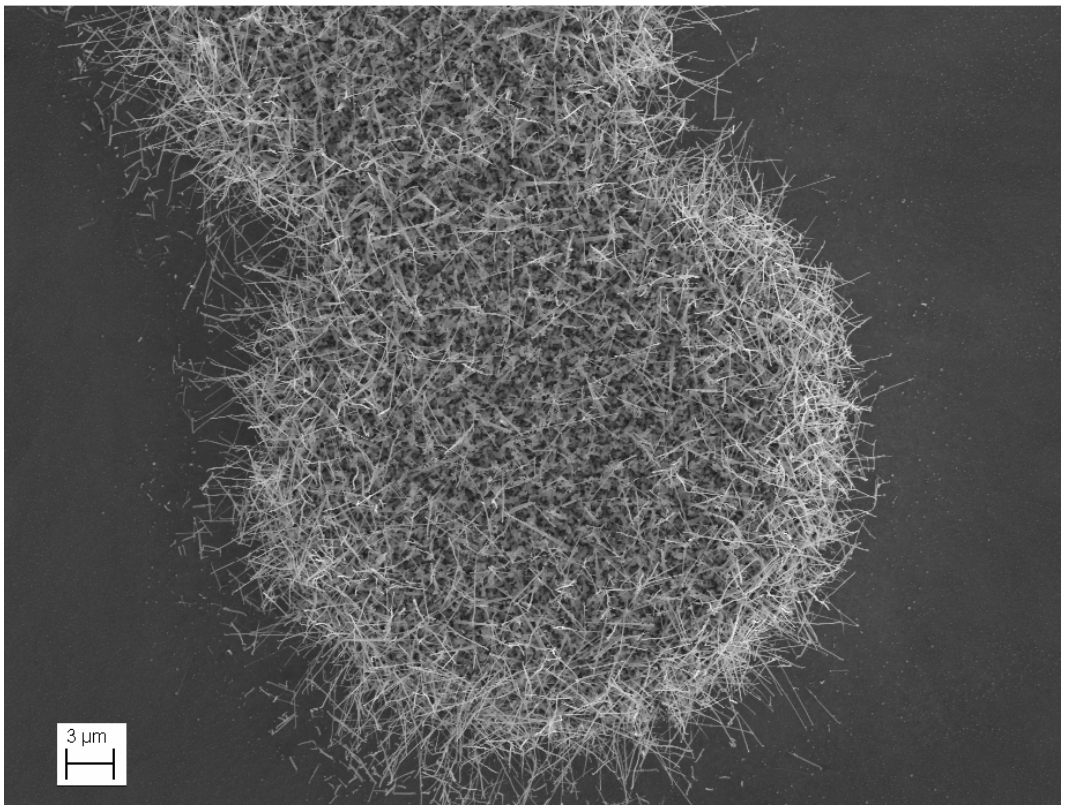

Figure 4.11: SEM image of tube furnace sample from March 18, 2009. The growth parameter being tested was the location of the sample relative to the source. This sample was face down on top of the source boat.

The SEM image in Figure 4.12 shows an island of ZnO nanowires, typical of the areas near the edge of the growth where the sample is not as bright white. These are possibly catalyzed by dust particles or some other type of contaminant.

Next, a photograph (Figure 4.12) and a SEM image (Figure 4.13) from the growth on March 19, 2009 will be discussed. The growth parameter that was changed in this experiment was again the location of the source relative to the sample. The powder was placed directly on the surface of the sample at the leading edge.

Figure 4.12: Photograph of tube furnace sample from March 19, 2009. The growth parameter being tested was the location of the sample relative to the source. This sample was face down on top of the source boat.

The photograph in Figure 4.12 shows that there was no growth in the area on the left edge of the sample where the powder was placed. The sample had between 25% and 50% nanowire coverage, and there was a visible decrease in the whiteness of the growth with distance from the leading edge.

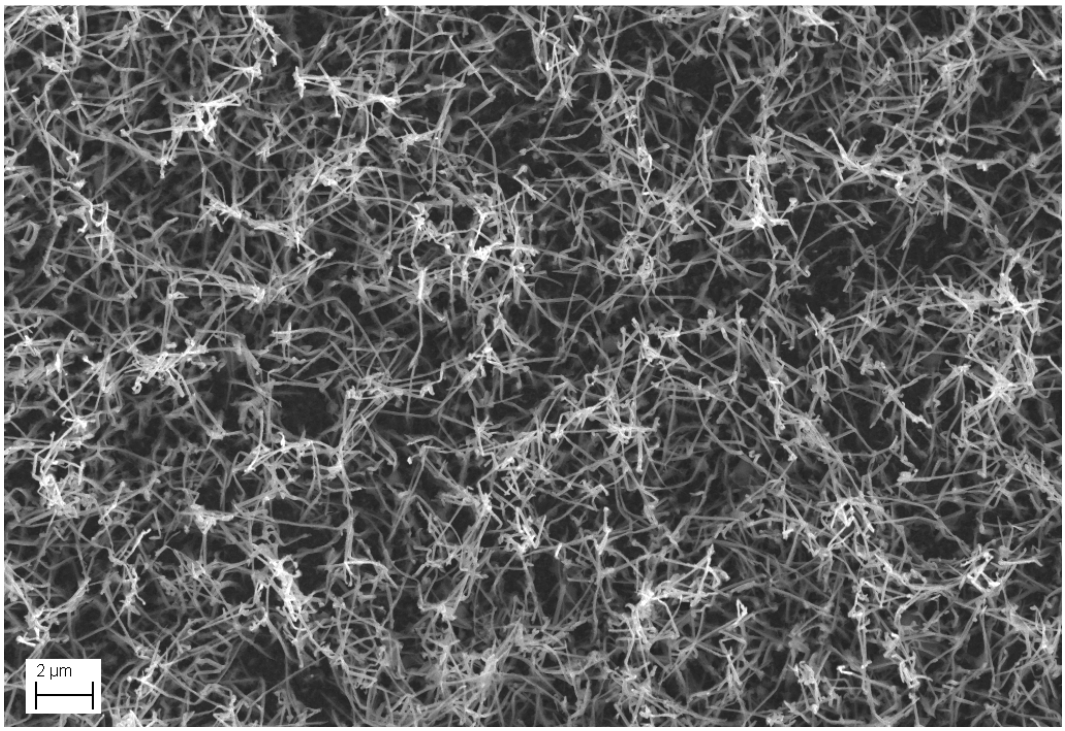

Figure 4.13: SEM image of tube furnace sample from March 19, 2009. The growth parameter being tested was the location of the sample relative to the source. This sample was face down on top of the source boat.

The SEM image in Figure 4.13 shows high density nanowire growth. This is representative of the whitest areas of the sample. These nanowires are under 500 nm in diameter and over 1 µm in length.

The next sample is the first sample from Run 1 on April 10, 2009. The important growth parameter for this sample was Ar flow rate. The Ar flow rate for this growth was 3.3 L/min. This sample was immediately downstream of the source boat. The photograph is shown in Figure 4.14, and the SEM image is shown in Figure 4.15.

Figure 4.14: Photograph of tube furnace Sample 1 from Run 1 on April 10, 2009. The important growth parameter in this experiment was Ar flow rate, which was 3.3 L/min.

The photo in Figure 4.14 shows nearly 50% coverage on the upstream half of the sample, but the visible growth is a very dull white-grey color and not the desirable bright white.

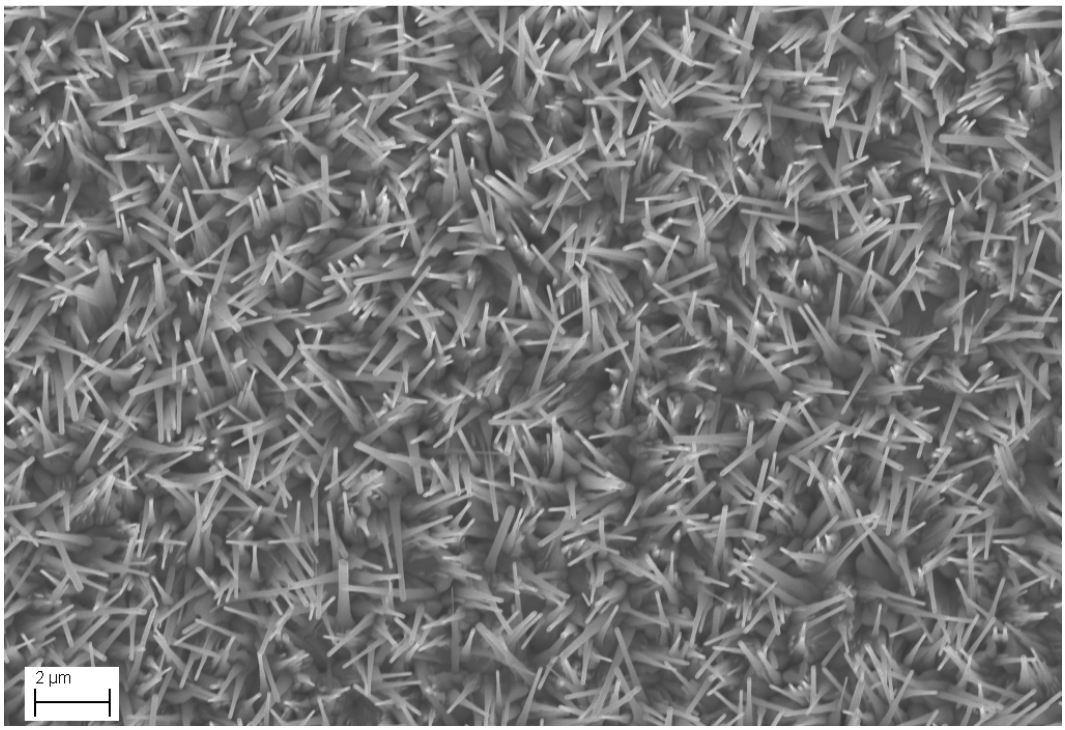

Figure 4.15: SEM image of tube furnace Sample 1 from Run 1 on April 10, 2009. The important growth parameter in this experiment was Ar flow rate, which was 3.3 L/min.

The SEM image in Figure 4.15 shows nanowires that are under 200 nm in diameter and around 2 μm in length. These nanowires are the best nanowires from this sample, and they are not typical of the entire area where growth occurred. The rest of the sample where growth occurred had some very low aspect ratio nanowires and amorphous chunks of material. On the downstream half of the sample, almost no growth was observable using SEM. The high Ar flow rate probably purged O_2 from the quartz tube well enough that we can conclude that O_2 is unnecessary for growth.

4.1.3 Other Results

There are suggestions in the literature (Hejazi, Hosseini and Ghamsari 2008) that CO_2 produced in the carbothermal reaction of the source material may contribute to the downstream oxidation reactions that create ZnO nanowires. The effectiveness of CO2 as an oxidizer was investigated. Results from both runs on April 2, 2009 were done in a CO_2 atmosphere instead of an Ar atmosphere, and no nanowire growth was observed whatsoever. The photo of the sample from the first run with CO_2 atmosphere is shown in Figure 4.17.

Figure 4.16: Photograph of tube furnace sample from April 2, 2009. This growth was performed in a CO_2 atmosphere.

Under these same conditions with Ar as the atmosphere gas, some nanowire growth was observed on March 13 and March 19. According to Le Chatelier's principle, increasing the concentration of a reactant species without changing the concentration of other

reactant species necessarily increases reaction rate (Kee, Coltrin and Glarborg 2003). This indicates that CO_2 does not contribute to the reactions that produce the nanowire growth because an increase in reaction rate would not result in samples that appear bare. This is supported by the lack of adsorption of CO_2 molecules on Au particle surfaces (Pansare, Sirijaruphan and Jr. 2005).

4.2 BENCH-TOP FURNACE

4.2.4 Bench-top Furnace Photos Paired with SEM Results

The results from the tube furnace suggested that good nanowire growth conditions were correlated with a close proximity between the source material and the sample and that surrounding flow conditions were of lesser importance. For this reason it was decided to experiment with growing nanowire samples using a closed bench-top furnace. The bench-top furnace was simpler and easier to operate than the tube furnaces. The first results presented here were from the first successful bench-top furnace growth from the first run on May 29, 2009. The sample was placed face down directly on top of a 2 inch source boat, and both were placed in the top portion of the stainless steel chamber. The growth duration was 30 minutes at a set point of 920ºC. During the growth process one of the end-caps that normally sealed the stainless steel chamber fell off, allowing more than usual air contact with the sample. The photograph is shown in Figure 4.17 and the SEM images are shown in Figure 4.18, Figure 4.19, and Figure 4.20.

Figure 4.17: Photograph of bench-top furnace sample from Run 1 of May 29, 2009. This sample was placed face down on the 2 inch source boat inside the open stainless steel chamber.

The photograph in Figure 4.17 shows that there is 50% to 75% nanowire coverage, but if only the area that was directly over the boat is considered, the coverage is nearly 100%. This sample appeared 3-dimensional without any magnification. The microwires in the whitest areas were visible to the naked eye. There is somewhat less dense coverage in the middle of the sample, no microwires were visible here.

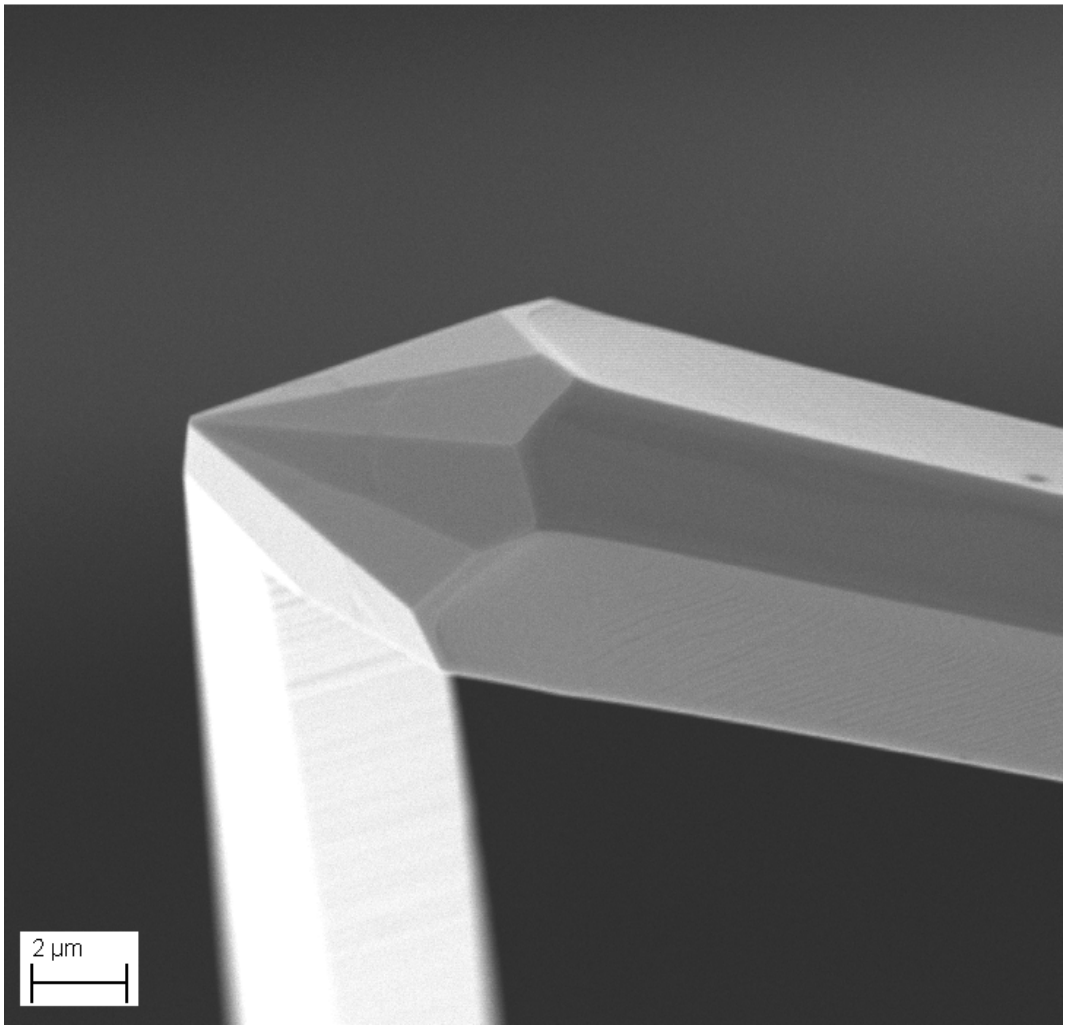

Figure 4.18: SEM image of bench-top furnace sample from Run 1 of May 29, 2009. This sample was placed face down on the 2 inch source boat inside the open stainless steel chamber. Large size and faceted appearance indicate VS growth, also known as self-catalysis.

The image in Figure 4.18 shows a good example of faceted growth discussed in Kumar et al., 2008. This is indicative of VS growth, also known as self-catalysis. This microwire is also much too large to have formed by the VLS mechanism at nearly 5 µm in diameter and over 1 mm in length.

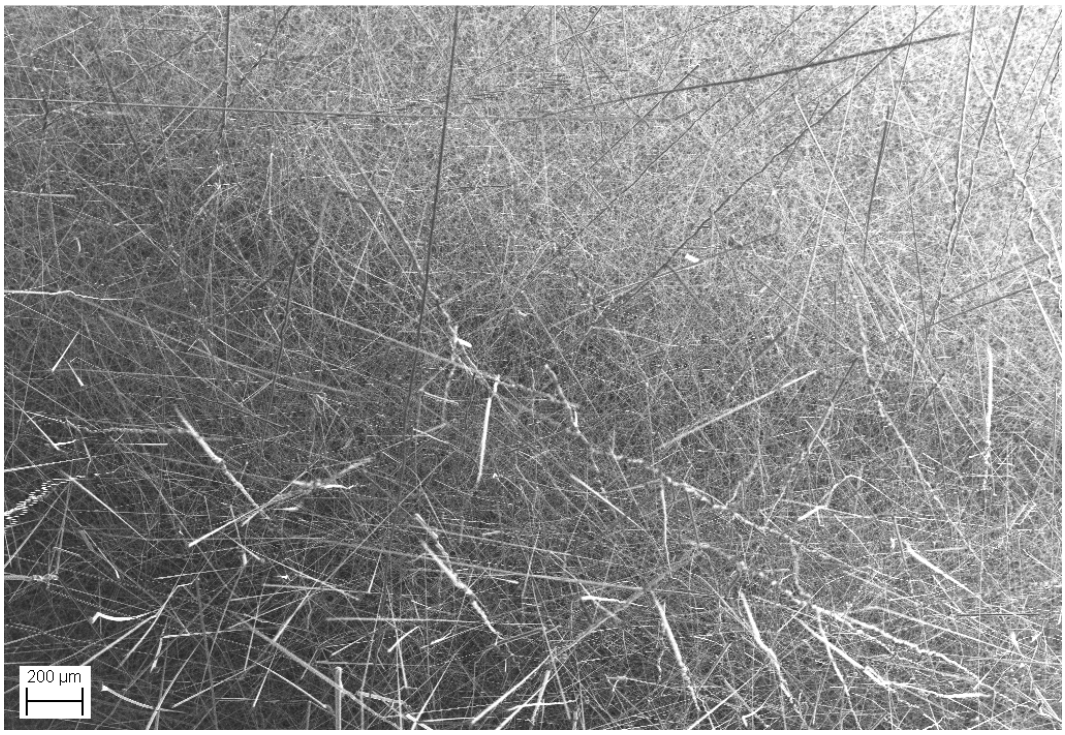

Figure 4.19: SEM image of bench-top furnace sample from Run 1 of May 29, 2009. This sample was placed face down on the 2 inch source boat inside the open stainless steel chamber. This image was taken at the minimum magnification available on the Supra SEM in the same location as the image shown in Figure 4.18.

The SEM image in Figure 4.19 was taken in the same location as the image shown in Figure 4.18, but this image was taken with the minimum usable magnification of the Supra SEM. All of the microwires shown in this image are roughly the same size as the one shown in the previous figure.

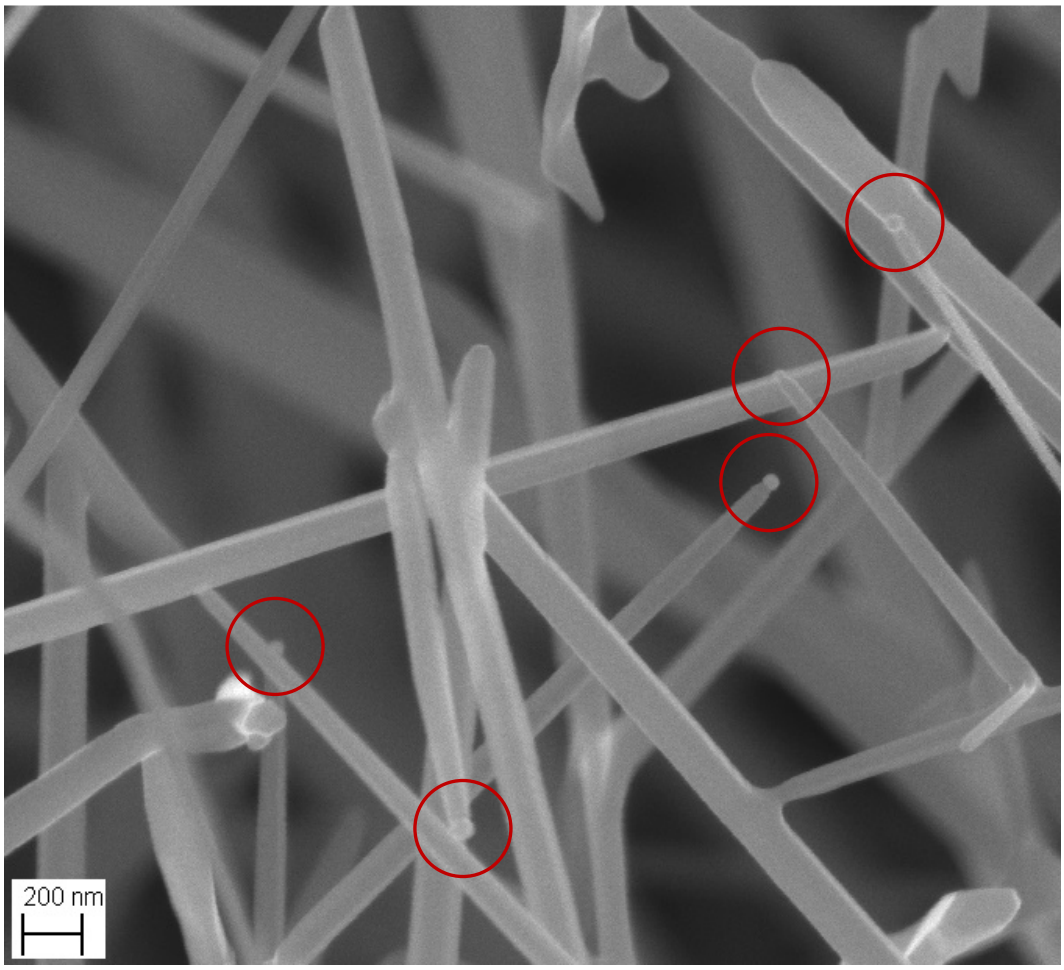

Figure 4.20: SEM image of bench-top furnace sample from Run 1 of May 29, 2009. This sample was placed face down on the 2 inch source boat inside the open stainless steel chamber. Gold catalyst tips are circled in red.

Figure 4.20 shows several nanowires with gold tips (circled in red) of similar diameter to the wires themselves. Note that the wires are not faceted and have nearly the same diameter as the gold tips. This is indicative that the VLS growth mechanism was actually occurring here.

The next growth was in a quartz Petri dish rather than inside the stainless steel chamber. The bottom of the dish was covered with a roughly 5 mm thick layer of mixed graphite and ZnO powder. The sample was placed face down on two small pieces of Si

at either end about 1 mm above the powder. The temperature set point was 1000ºC for this growth, and the growth duration was 10 minutes. The photograph of the sample and two SEM images are in Figure 4.21Figure 4.24.

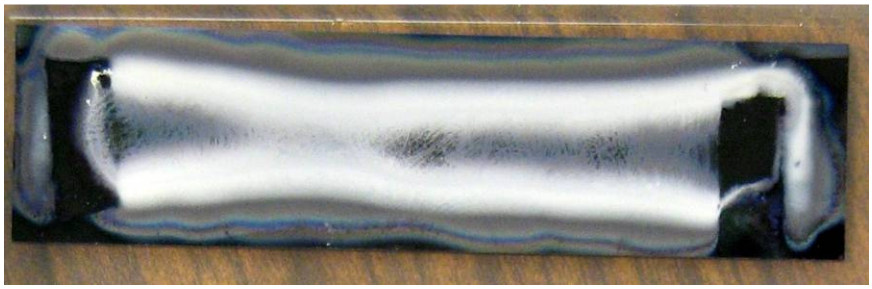

Figure 4.21: Photograph of bench-top furnace sample from Run 2 of May 29, 2009. This sample was placed face down on two Si supports that held it about 1 mm above the powder in the quartz Petri dish.

Figure 4.21 shows that more of the sample was exposed to the vapors, and this sample was 50% to 75% covered with nanowires. However, there was as large area in the middle of the sample with sparse nanowire coverage due to the short growth duration. Microwires were not visible to the unaided eye.

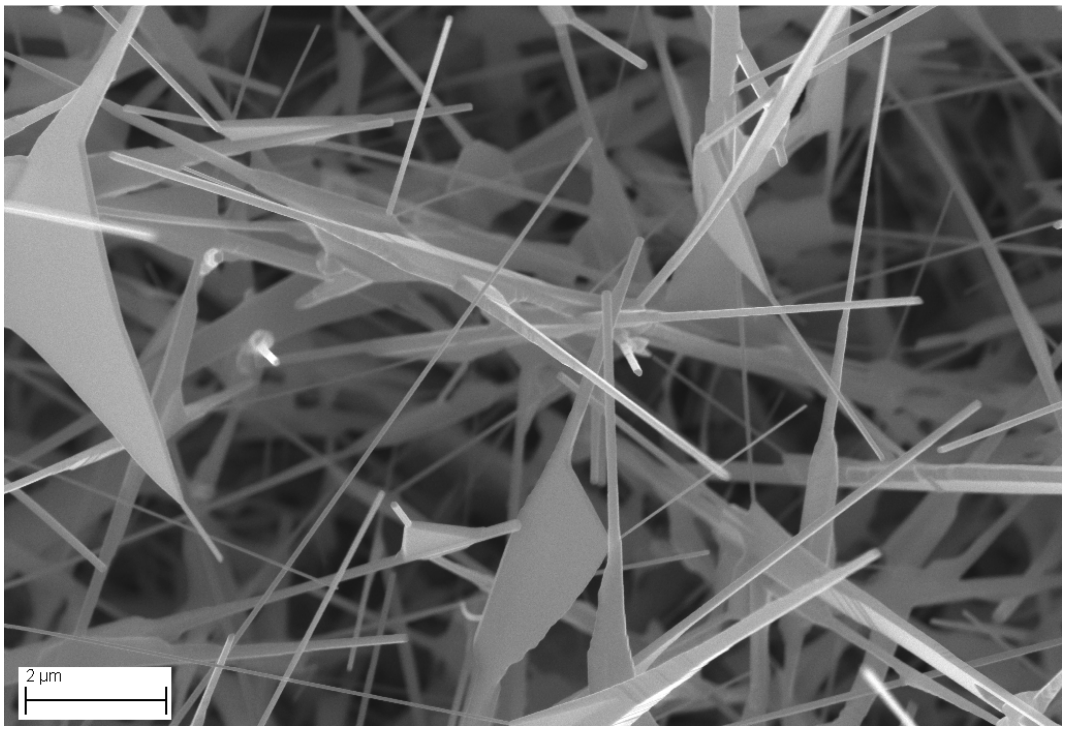

Figure 4.22: SEM image of bench-top furnace sample from Run 2 of May 29, 2009. This sample was placed face down on two Si supports that held it about 1 mm above the powder in the quartz Petri dish.

Figure 4.22 shows 1-dimensional nanowires and 2-dimensional plate-like structures. These plate-like structures are approximately 200 nm thick with an area on the order of 5 μm^2.

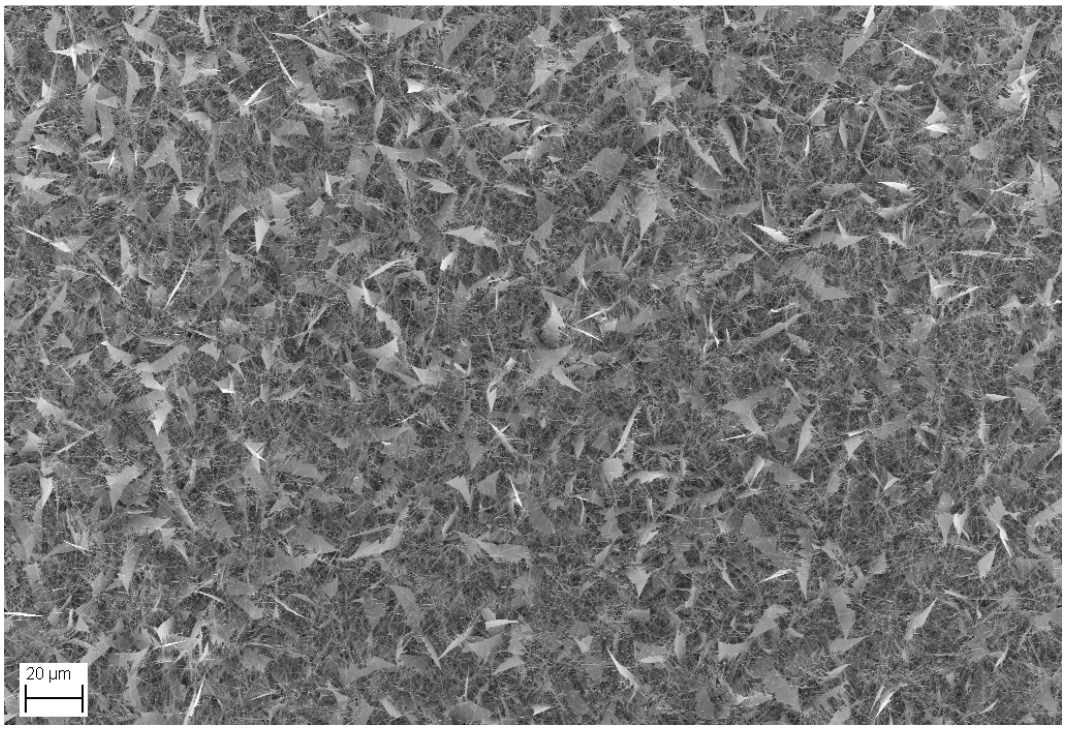

Figure 4.23: SEM image of bench-top furnace sample from Run 2 of May 29, 2009. This sample was placed face down on two Si supports that held it about 1 mm above the powder in the quartz Petri dish. This image was taken from the same location as the image shown in Figure 4.22.

Figure 4.23 is an image that was taken from the same location as the image in the previous figure with much lower magnification. This image shows an area on the order of 1 mm^2 densely covered with nanowires and plate-like structures.

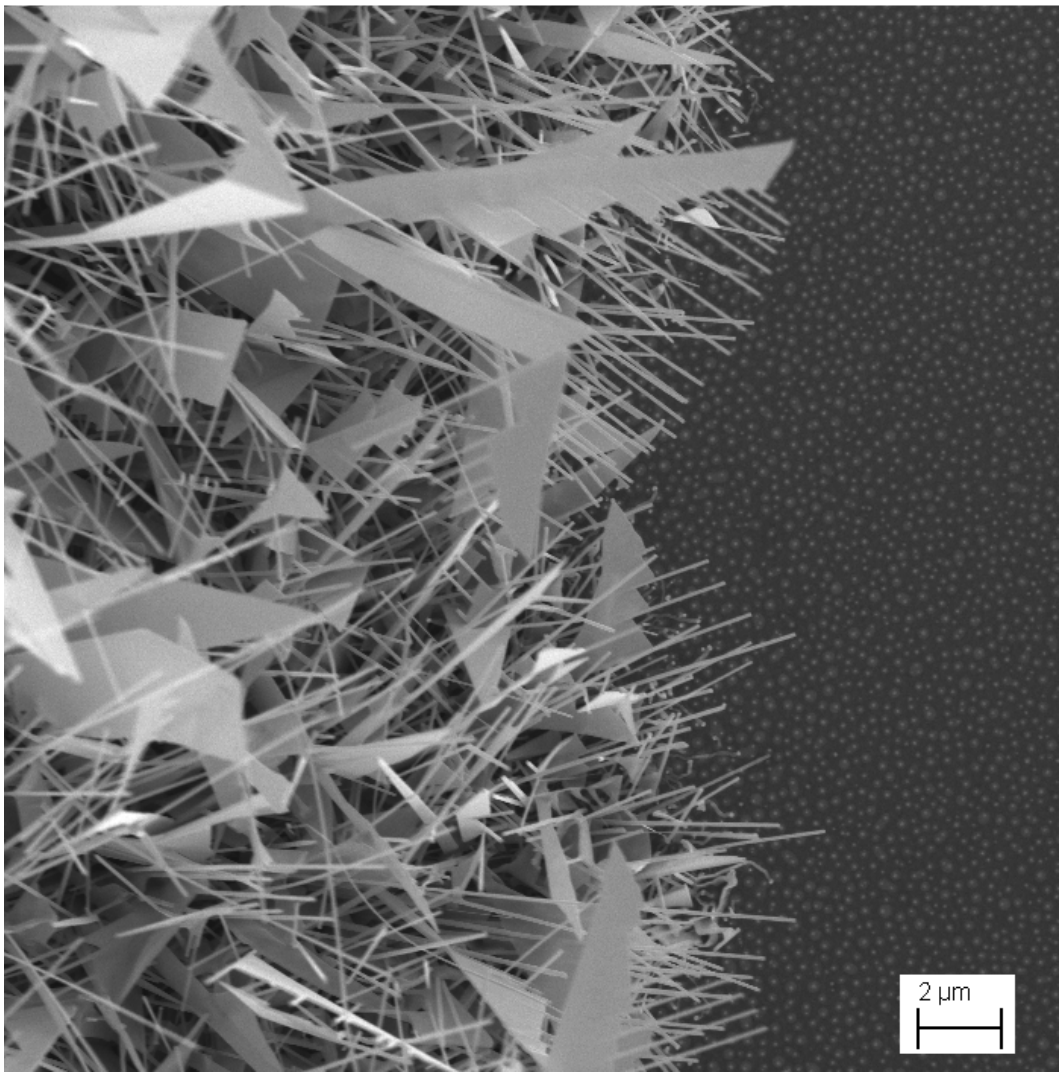

Figure 4.24: SEM image of bench-top furnace sample from Run 2 of May 29, 2009. This sample was placed face down on two Si supports that held it about 1 mm above the powder in the quartz Petri dish. Nanocombs and nanowires are visible here.

The SEM image in Figure 4.24 shows both nanowires and nanocombs. This image was taken at the edge of a white area where there was a distinct line separating areas with and without growth.

These first bench-top furnace growths were still not as uniform as we wanted them to be so we spent some time thinking about what mechanism might be causing this.

Based on the photos in Figure 4.17 and Figure 4.21, it appears that the diffusion process produces a reaction front that is analogous to a diffusion flame. Zn vapor, the equivalent species to the fuel, diffuses outward from the center of the sample, and O_2, the oxidizer, diffuses inward. It is unlikely that CO produced by the carbothermal reaction is substantially contributing to this diffusion flame-like growth because CO vapor would be pre-mixed with Zn vapor since they are produced by the same source. Also, nanowire growth was much less dense in the stainless steel chamber when it was sealed from the outside air. Based on previous experiments in the tube furnace, it seemed implausible that CO_2 could contribute to this growth. Based on the success of run 1 of May 29 when the sample was placed face down on a 2 inch source boat, we wanted to design a source boat large enough to expose the entire sample to the source powder. This led us to design the boat with beams shown in Figure 2.12. The side walls of the boat would hold the sample in place and limit the rate of diffusion of O_2 under the sample.

The next two growths from June 11 and June 17, 2009 were the first to use the boats with beams. Both growths used a set point of 1000ºC. The June 11 growth had a growth duration of 30 minutes, and the June 17 growth had a growth duration of 60 minutes. The results of these growths are shown in the images in Figure 4.25 and Figure 4.27, respectively. The corresponding SEM images are shown in Figure 4.26Figure 4.29.

Figure 4.25: Photograph of bench-top furnace Sample 1 from June 11, 2009 growth. This sample was face down on the beams of the quartz boat for 30 minutes. This was the first sample to use the quartz boat. The powder was loose just below the beams. Shadows can be seen were the beams were blocking diffusion to the sample.

Figure 4.25 shows greater than 75% coverage. This indicates that our method of using diffusion transport without forced convection worked well. There were microwires in the whitest areas, and there was some appearance of 3-dimensional texture visible to the unaided eye. To our knowledge, this is the most successful uniform, large scale coverage that has been achieved by any group. This is also the first attempt of any group at growth outside a quartz tube with no control of the species in the atmosphere.

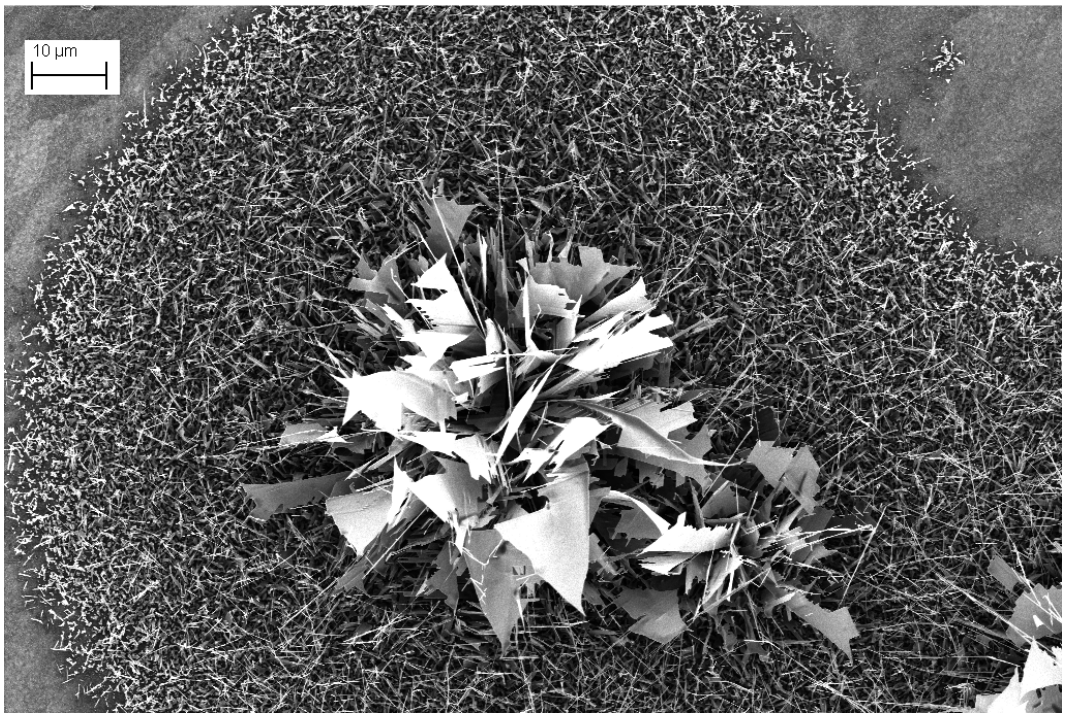

Figure 4.26: SEM image of bench-top furnace Sample 1 from June 11, 2009 growth. This sample was face down on the beams of the quartz boat for 30 minutes. This was the first sample to use the quartz boat. The powder was loose just below the beams. This image was an island in the area that was shadowed by the beam of the boat.

The island of growth shown in Figure 4.26 shows large plate-like structures that are several microns squared in area. It is not possible to obtain a good estimate of the thickness of these structures with this magnification. There are also high aspect ratio nanowires shown with lengths over 10 µm and diameters that are under 500 nm.

Figure 4.27: Photograph of bench-top furnace sample from June 17, 2009 growth. This sample was face down on the beams of the quartz boat for 60 minutes. The powder was loose just below the beams.

Figure 4.27 shows a growth with greater than 75% coverage. As stated above, the only change from June 11 to June 17 was increasing the growth time from 30 minutes to 60 minutes. The source powder appeared mostly white at the end of the growth, indicating that graphite oxidation was competing with the carbothermal reaction. Since there was almost no graphite left, no Zn, CO, and CO_2 vapor was being produced near the end of the growth. This growth didn't show much improvement over the previous growth, probably because the Zn vapor was no longer produced as the graphite was burned away by oxidation.

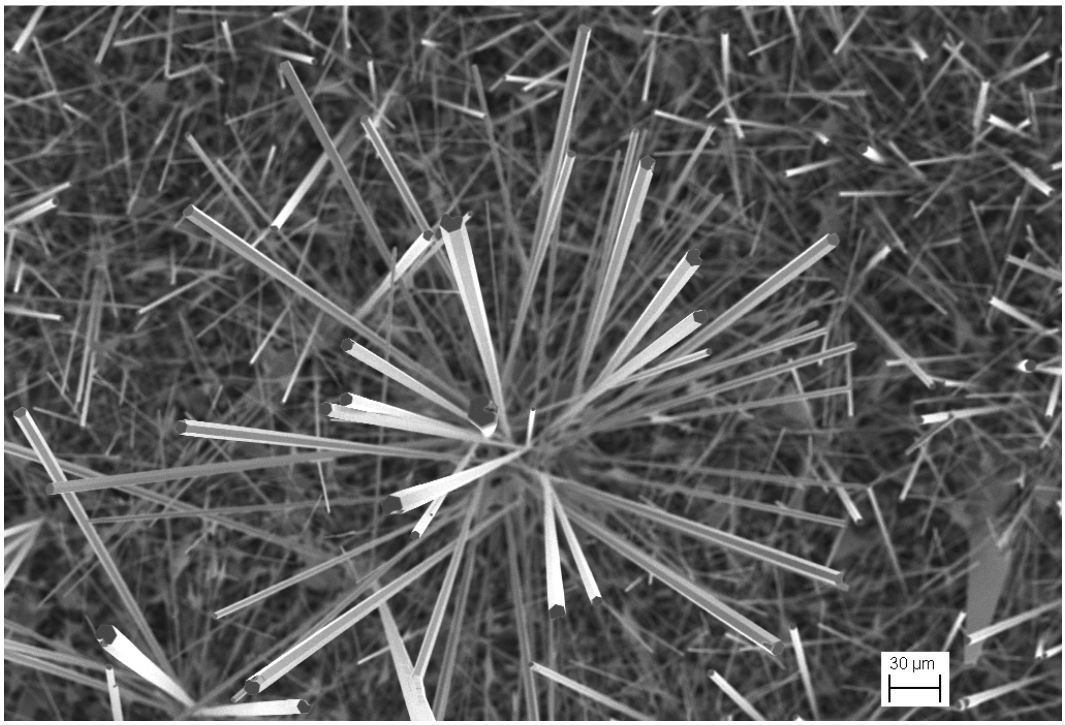

Figure 4.28: SEM image of bench-top furnace sample from June 17, 2009 growth. This sample was face down on the beams of the quartz boat for 60 minutes. The powder was loose just below the beams. Microwires are in the foreground, and nanowires are in the background.

Figure 4.28 shows microwires that were nearly vertical so the magnitude of their length was not apparent in this image. Based on focal distance, these microwires must have been several hundred microns in length, and they were around 10 µm in diameter. These microwires had no Au tips and were grown by the VS mechanism. High aspect ratio nanowires are shown in the background.

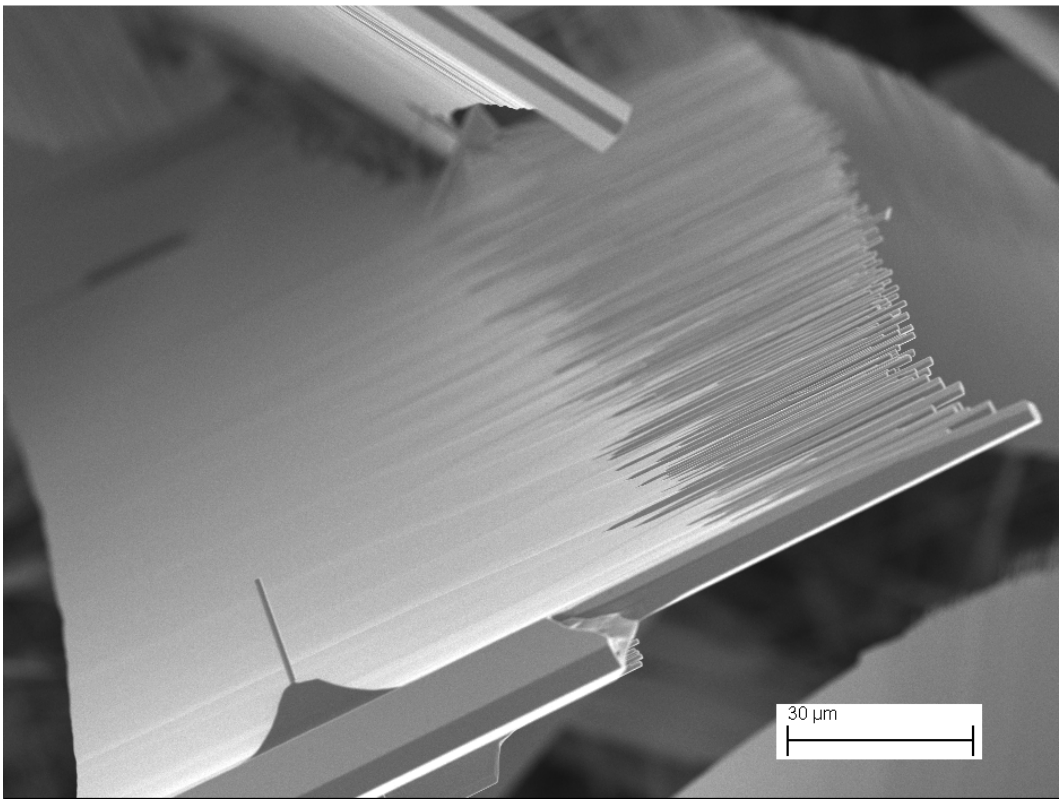

Figure 4.29: SEM image of bench-top furnace sample from June 17, 2009 growth. This sample was face down on the beams of the quartz boat. The powder was loose just below the beams.

Figure 4.29 shows a massive structure that resembles either a nanocomb or a nanoribbon. The area of this structure was on the order of 0.01 mm^2. The structure was approximately 10 µm in thickness. In both of the growths in the boat with beams discussed so far, there was no apparent decrease in nanowire areal density where microwires were also present.

The June 12 growth was intended to test whether the presence of catalyst metal mattered for the effectiveness of the growth. The growth parameters were similar to those used on June 11 with two changes. There was no catalyst metal, and the growth duration was 15 minutes instead of 30 minutes. The photograph of the sample and the SEM image are shown in Figure 4.30 and Figure 4.31.

Figure 4.30: Photograph of bench-top furnace sample from June 12, 2009. This sample was face down on the beams of the boat. There was no catalyst layer on this sample.

Figure 4.30 shows some nanowire growth, but the middle of the sample is largely void. There is between 25% and 50% coverage. This sample is a good example of the diffusion flame-like behavior of the reaction front produced by nanowire growth in the boat with beams.

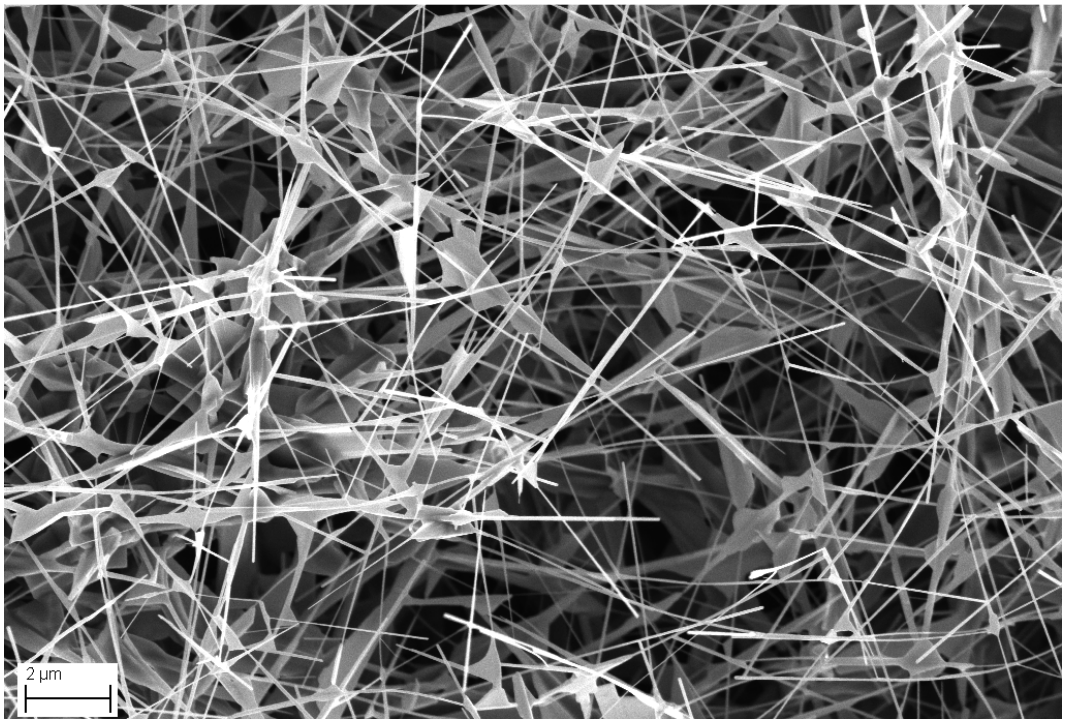

Figure 4.31: SEM image of bench-top furnace sample from June 22, 2009. This sample was face down on the beams of the boat. There was no catalyst layer on this sample.

There was no tip growth found on this sample, and many of the nanostructures had a faceted appearance. Because there was no catalyst to cause VLS growth, all of the growth shown in Figure 4.31 was VS growth. This indicates that no catalyst was necessary to initiate VS growth. However, it cannot be concluded that VS growth can never initiated by a catalyst. It is feasible that VLS growth could be the initial growth mechanism with VS growth taking over as source vapor species flux to the surface of the sample increases when a catalyst is present.

4.2.5 Other Bench-top Furnace Results

The 5 runs on July 3 progressed by changing one variable at a time. In the first four runs, that variable was the powder profile. A schematic illustrating the effects of powder profile is shown in Figure 4.36 as a cross-section view of the boat with beams. The schematic also clarifies what is meant by powder profile. The first run had a slightly concave powder profile. The second run had a large convex profile. The third run had a large concave profile, and the fourth and fifth runs had a large concave profile. Also, powder was used to cover a small gap between the edge of the sample and the walls of the boat in the fourth and fifth runs. In the fifth run, all growth parameters were identical to the fourth run except Cu was used as the metal layer instead of Au. All of these growths had 2.5 nm of catalyst metal, a temperature set point of 1000ºC, and a growth duration of 15 minutes. The fourth run was accidentally left in the furnace an extra two minutes, resulting in a 17 minute growth duration. All the July 3 growths were done in the boat with beams. The photographs of the samples from these growths are shown in Figure 4.32 to Figure 4.37.

Figure 4.32: Photograph of bench-top furnace sample from Run 1 on July 3, 2009. This sample was face down on the beams of the boat. The powder was thoroughly packed and then scraped to have a slightly concave upward profile.

Figure 4.32 shows diffusion flame-like behavior, with a sparse growth area in the middle of the sample. The growth was likely O_2 limited in the middle due to the competing diffusion counterflow of Zn vapor in the outward direction.

Figure 4.33: Photograph of bench-top furnace sample from Run 2 on July 3, 2009. This sample was face down on the beams of the boat. The powder was thoroughly packed and then scraped to have a large convex upward profile.

Figure 4.33 shows an even worse sparse area in the middle of the sample than the previous growth. The convex profile likely increased the diffusion flow rate of Zn vapor outward from the middle of the sample, thus preventing O_2 from effectively oxidizing Zn in this area. The region of dense growth appears to have narrowed from the outside also. This is likely due to an excessive concentration of O_2 in this region. The distance between the sample and powder is larger near the outside of the sample so the diffusion flow velocity of the Zn vapor would decrease in this region. It is possible that Zn was being oxidized in the gas phase as well. This would compete with nanowire growth.

Figure 4.34: Photograph of bench-top furnace sample from Run 3 on July 3, 2009. This sample was face down on the beams of the boat. The powder was thoroughly packed and then scraped to have a large concave upward profile.

Figure 4.34 shows a drastic improvement over the previous growth. The large concave powder profile must increase the uniformity of species concentration over the surface of the sample.

Figure 4.35: Photograph of bench-top furnace sample from Run 4 on July 3, 2009. This sample was face down on the beams of the boat. The powder was thoroughly packed and then scraped to have a slightly concave upward profile. Powder was placed on top of the sample to cover a small gap between the side walls of the boat and the edge of the sample.

Figure 4.35 shows a further improvement over the previous growth. During the previous growth, we observed a small gap between the side walls of the boat and the edge of the sample. This gap was collocated with the curve in the bottom of the image in Figure 4.34 so we thought it might be allowing Zn vapor out from under the sample too easily or that it was allowing O_2 under the sample too easily. By covering it over with ZnO+C powder, we were able to eliminate the curve.

Based on the results shown in figures, we have prepared a schematic representation of powder profile and its effects shown in Figure 4.36.

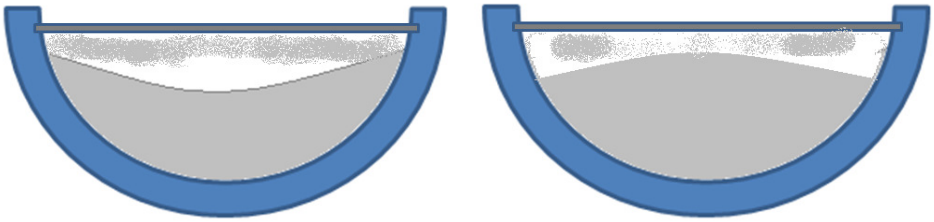

Figure 4.36: Schematic of cross-section of source boat with beams for concave powder profile (left) and convex powder profile (right). Vapor concentrations are illustrated by gray, smoke-like illustration. Darker regions represent better mixing of Zn vapor and O_2. These dark regions correspond to the growth region.

As shown in Figure 4.36, the concave powder profile resulted in a broader growth region than did the convex powder profile. The convex powder profile had dense growth, but only over a narrow band. The convex powder profile resulted in now growth in the middle of the sample. The inner region of the sample was O_2 starved, and the outer region was Zn vapor starved, much like a diffusion flame. The concave profile allowed more inward diffusion of O_2 and more outward diffusion of Zn.

Figure 4.37: Photograph of bench-top furnace sample from Run 5 on July 3, 2009. This sample was face down on the beams of the boat. The powder was thoroughly packed and then scraped to have a slightly concave upward profile. This sample was coated with 2.5 nm of Cu instead of Au.

Figure 4.37 shows results from the use of Cu catalyst material. It gave poor growth with approximately 25% coverage. This growth is similar in appearance to the growth with no catalyst layer. This indicates that Cu is not as effective at catalyzing

nanowire growth as Au. This also suggests that the faceted nanowires grown by Li, Lee and Tseng (2003) with a Cu catalyst layer were not grown by the VLS mechanism. The faceted nanowires in their work and our poor success with Cu lead us to believe that their nanowires would have grown by the VS mechanism without the presence of Cu.

Chapter 5: Conclusions and Recommendations

5.1 Conclusions

5.1.1 Tube Furnace

Several types of nanostructures were grown in the tube furnace. However, the goal was to achieve uniform coverage over an entire sample, and this did not happen in the tube furnace. Vapor phase transport growth of ZnO nanowires has been demonstrated successfully many times in literature, but none of the groups explicitly reported uniform coverage over a large area. This is likely due to the fact that large scale coverage is not needed for fabrication of the types of devices in which these nanowires are typically used.

While O_2 does contribute to ZnO nanowire growth, it is seemingly unnecessary. In experiments where extra effort was made to remove all O_2 from the quartz tube, nanowire growth was still achieved.

According to this research and supporting evidence in literature, CO_2 does not contribute to nanowire growth. Using an atmosphere composed entirely of CO_2, no nanowire growth was observed. According to Le Chatelier's Principle, increasing the concentration of a proposed reactant, CO_2 in this case, should increase the reaction rate. Since the opposite happens, it must be concluded that CO_2 is a non-participating diluent. Additionally, Pansare, Sirijaruphan and Jr. 2005 have shown that CO_2 does not adsorb on solid Au nanoparticles, indicating that CO_2 cannot contribute to VS growth.

5.2 Bench-top Furnace

The small distance between the source and sample and lack of forced flow in the bench-top furnace increase the concentration of Zn vapor, ZnO vapor, and CO vapor to which the sample was exposed. The surface profile of the powder enabled further tuning

of species concentrations, and these conditions offered substantial improvement over the tube furnace growths in which they were not adjustable.

VS growth can occur without an effective catalyst as seen on the sample with no catalyst layer and the sample with a Cu metal layer. VS growth can also occur in conjunction with VLS growth, and VLS growth likely leads to VS growth if reactant species flux to the sample surface is greater than the catalytic reaction rate that produces nanowire growth. It is clear that VLS growth can occur only if a layer of Au catalyst is present, but it is unclear which vapor species contribute to VLS growth. There are several possible reaction pathways by which vapor species can contribute to nanowire growth. Adsorbed Zn atoms might be oxidized by adsorbed CO molecules. Adsorbed Zn atoms might be oxidized by adsorbed O atoms. Vapor phase ZnO might be adsorbing and contributing directly to nanowire growth. Vapor phase ZnO might be produced by Zn oxidizing with O_2 or CO, and/or vapor phase ZnO might be directly evaporating from the source powder. It is currently unknown which, if not all, of these reactions can contribute to VLS growth.

5.3 RECOMMENDATIONS

For all methods and conditions in this study, little is understood about which growth species contribute to the VS mechanism and which growth species contribute to the VLS mechanism. To learn more about the chemical reaction pathways and kinetics in the tube furnace, a CO atmosphere should be used to determine how CO contributes to the growth. The boat with beams should also be used in the tube furnace with varying concentration O_2 injection to see how this affects the shape of the reaction front.

Little is understood about which vapor phase species contribute to the VLS mechanism and which vapor phase species contribute to the VS mechanism. Due to an

impending deadline, no further research has been completed to clarify this. Experiments with and without catalyst layers should be tried with ZnO+C powder and ZnO only powder to determine which vapor species out of Zn, ZnO, CO, and O_2 are contributing to VLS growth. If this enables us to determine which species contribute to VLS growth, it should be possible to tune the reactions to produce only VLS growth. This would be desirable because it would eliminate the other types of structures which have smaller specific areas. To test the effect of completely removing O_2 from the reactions, the sample could be completely buried in powder. This should be tested in conjunction with the other tests.

In addition, upon determining how the reactant species contribute to VLS growth and VS growth, the effects of powder profile, vapor phase reaction rates, surface reaction rates, and species diffusion should be modeled for the boat with beams. This would potentially enable better tuning of the powder profile.

Appendix A: Growth Parameters

A.1 Tube Furnace Growth Parameters

Date	Run	Catalyst Thickness (nm)	Downstream Furnace Setpoint (°C)	Upstream Furnace Setting	Annealing Time (min)	Growth Duration (min)	Main Gas	Main Flow Regulator	Flow Rate
1/26	1	2.0	900	0	0	20	Ar	electronic	25 sccm
1/27	1	2.0	900	0	0	8	Ar	electronic	25 sccm
1/28	1	2.0	800	0	0	20	Ar	electronic	25 sccm
1/28	2	2.0	900	0	0	1	Ar	electronic	25 sccm
2/4	1	2.0	900	5	0	60	Ar	rotameter 18 plastic	50 mL/min
2/4	1	50.0	900	5	0	60	Ar	rotameter 18 plastic	50 mL/min
2/4	1	10.0	900	5	0	60	Ar	rotameter 18 plastic	50 mL/min
2/11	1	2.0	900	5	0	60	Ar	rotameter 18 plastic	50 mL/min
2/11	1	50+	900	5	0	60	Ar	rotameter 18 plastic	50 mL/min
2/11	1	2.0	900	5	0	60	Ar	rotameter 18 plastic	50 mL/min
2/11	1	2.0	900	5	0	60	Ar	rotameter 18 plastic	50 mL/min
2/12	1	5.0	900	5	30	60	Ar	electronic	9 sccm

2/12	1	5.0	900	5	0	60	Ar	rotameter 18 plastic	50 mL/min
2/17	1	20.0	912	5	30	60ish	Ar	rotameter 90	25 mL/min
2/19	1	2.5	900	5	20	60	Ar	rotameter 90	25 mL/min
2/20	1	2.5	900	5	30	60	Ar	rotameter 90	50 mL/min
3/4	1	2.5	912	5	30	60	Ar	rotameter 90	24 mL/min
3/5	1	5.0	912	5	30	60	Ar	rotameter 90	24 mL/min
3/6	1	2.5	800	5	30	60	Ar	rotameter 90	24 mL/min
3/9	1	2.5	800	5	30	60	Ar	rotameter 90	24 mL/min
3/11	1	2.5	900	5	30	60	Ar	rotameter 90	64 mL/min
3/13	1	2.5	900	5	n/a	30	Ar	rotameter 90	24 mL/min
3/13	2	2.5	900	5	n/a	30	Ar	rotameter 90	24 mL/min
3/13	3	2.5	900	5	n/a	30	Ar	rotameter 90	24 mL/min
3/18	1	2.5	900	5	n/a	30	Ar	rotameter 90	24 mL/min
3/19	1	2.5	900	5	n/a	30	Ar	rotameter 90	25 mL/min
3/23	1	2.5	900	5	n/a	30	Ar	rotameter 90	25 mL/min

4/2	1	2.5	900	5	n/a	30	Ar	rotameter 90	25 mL/min
4/2	2	2.5	900	5	n/a	30	CO_2	rotameter 90	25 mL/min
4/2	3	2.5	900	5	n/a	30	CO_2	rotameter 90	25 mL/min
4/2	4	2.5	900	5	n/a	30	Ar	rotameter 90	25 mL/min
4/8	1	2.5	900	Hi (1200ºC)	n/a	30	Ar	rotameter 98	3300 mL/min
4/9	1	2.5	900	5	n/a	30	Ar/Air	rotameter 98	3300 mL/min
4/10	1	2.5	900	5	n/a	30	Ar	rotameter 98	mL/min
4/10	2	2.5	900	5	n/a	30	Ar	rotameter 98	-65 mL/min

Date	Run	$[O_2]$ (%)	Location of Sample	Location of Source
1/26	1	n/a	0.375" downstream from exit	adjacent to sample
1/27	1	n/a	0.375" downstream from exit	adjacent to sample
1/28	1	n/a	0.375" downstream from exit	adjacent to sample
1/28	2	n/a	0.375" downstream from exit	adjacent to sample
2/4	1	n/a	middle of downstream furnace	middle of upstream furnace
2/4	1	n/a	middle of downstream furnace	middle of upstream furnace
2/4	1	n/a	middle of downstream furnace	middle of upstream furnace
2/11	1	n/a	middle of downstream furnace	middle of upstream furnace
2/11	1	n/a	middle of downstream furnace	middle of upstream furnace
2/11	1	n/a	middle of downstream furnace	middle of upstream furnace
2/11	1	n/a	middle of downstream furnace	middle of upstream furnace
2/12	1	n/a	middle of downstream furnace	middle of upstream furnace
2/12	1	n/a	middle of downstream furnace	middle of upstream furnace
2/17	1	21%	middle of downstream furnace	middle of upstream furnace
2/19	1	21%	middle of furnace	adjacent to sample
2/20	1	21%	middle of downstream furnace	middle of upstream furnace
3/4	1	5%	middle of downstream furnace	middle of upstream furnace
3/5	1	5%	middle of downstream furnace	middle of upstream furnace
3/6	1	5%	middle of downstream furnace	middle of upstream furnace
3/9	1	5%	middle of downstream furnace	middle of upstream furnace

3/11	1	5%	middle of downstream furnace	middle of upstream furnace
3/13	1	n/a	face down on top of source	middle of downstream furnace
3/13	2	n/a	source and sample adjacent and centered in downstream furnace	
3/13	3	n/a	face up on top of source	middle of downstream furnace
3/18	1	n/a	face down on top of source	middle of downstream furnace
3/19	1	n/a	middle of furnace	powder directly on sample
3/23	1	n/a	middle of furnace	powder directly on sample
4/2	1	n/a	middle of furnace	powder directly on sample
4/2	2	n/a	source and sample adjacent and centered in downstream furnace	
4/2	3	n/a	face down on top of source	middle of downstream furnace
4/2	4	n/a	face down on top of source	middle of downstream furnace
4/8	1	n/a	one adjacent to source, one in middle of downstream furnace	84 cm upstream from exit
4/9	1	n/a	two downstream adjacent to source, one in middle of downstream furnace	84 cm upstream from exit
4/10	1	n/a	two downstream adjacent to source, one in middle of downstream furnace	84 cm upstream from exit
4/10	2	n/a	two downstream adjacent to source	84 cm upstream from exit

Table A.1: Comprehensive listing of tube furnace growth parameters.

A.2 Bench-top Furnace Growth Parameters

Run	Date	Catalyst Thickness (nm)	Catalyst Metal	Deposition Technique	Furnace Setpoint (°C)	Growth Duration (min)	Location of Sample	Location of Source
1	4/22/09	2.5	Au	Sputter*	920	30	center of petri dish	2 boats on either side of sample
2	4/22/09	2.5	Au	Sputter*	1000	30	center of petri dish	loose powder surrounding sample
1	4/23/09	2.5	Au	Sputter*	1000	30	face down ~1 mm above powder on Si supports	uniform layer in petri dish
2	4/23/09	2.5	Au	Sputter*	1000	30	face down center of petri dish	~1 mm underneath sample
1	5/26/09	2.5	Au	Sputter*	1000	60	bottom chamber of SS tube reactor	top chamber of SS tube reactor
1	5/28/09	2.5	Au	Sputter*	1000	60		
2	5/28/09	2.5	Au	Sputter*	1000	300		
1	5/29/09	2.5	Au	Sputter*	1000	60	top chamber of SS tube reactor face down on source boat	short boat in open top chamber of SS tube reactor beneath sample
2	5/29/09	2.5	Au	Sputter*	1000	10	center of petri dish	loose powder surrounding sample
1	6/1/09	2.5	Au	Sputter*	1000	60	top chamber of SS tube reactor face down on source boat	long boat in top chamber of SS tube reactor beneath sample
2	6/2/09	2.5	Au	Sputter*	1000	10		
1	6/3/09	2.5	Au	Sputter*	1000	60	face down in 5" long 22mm quartz tube	~1 mm underneath sample

1	6/5/09	2.5	Au	Sputter*	1000	10	top chamber of SS tube reactor face down on source boat	long boat in top chamber of SS tube reactor beneath sample. Flat powder surface.
2	6/5/09	2.5	Au	Sputter*	1000	10		long boat in top chamber of SS tube reactor beneath sample. Powder surface convex up.
1	6/11/09	2.5	Au	Sputter*	1000	30	face down on beams of boat	below beams of ~25 mm wide boat
2	6/12/09	0.0	Au	n/a	1000	15	face down on beams of boat	below beams of ~25 mm wide boat
1	6/17/09	2.5	Au	Sputter*	1000	60	face down on beams of boat	below beams of ~25 mm wide boat
1	6/22/09	2.5	Au	Sputter*	1000	10	face down on beams of boat	packed down with wafer and scraped to be even with beams
1	7/3/09	2.5	Au	Sputter*	1000	15	face down on beams of boat	scraped to have small concavity
2	7/3/09	2.5	Au	Sputter*	1000	15	face down on beams of boat	scraped to have large convexity
3	7/3/09	2.5	Au	Sputter*	1000	15	face down on beams of boat	scraped to have large concavity
4	7/3/09	2.5	Au	Sputter*	1000	17	face down on beams of boat	packed and scraped to have large concavity, covering gap on side of sample
5	7/3/09	2.5	Cu	Sputter*	1000	15	face down on beams of boat	

Table A.2: Comprehensive listing of bench-top furnace growth parameters

Appendix B: Calibration Plots

B.1 Rotameter Calibration

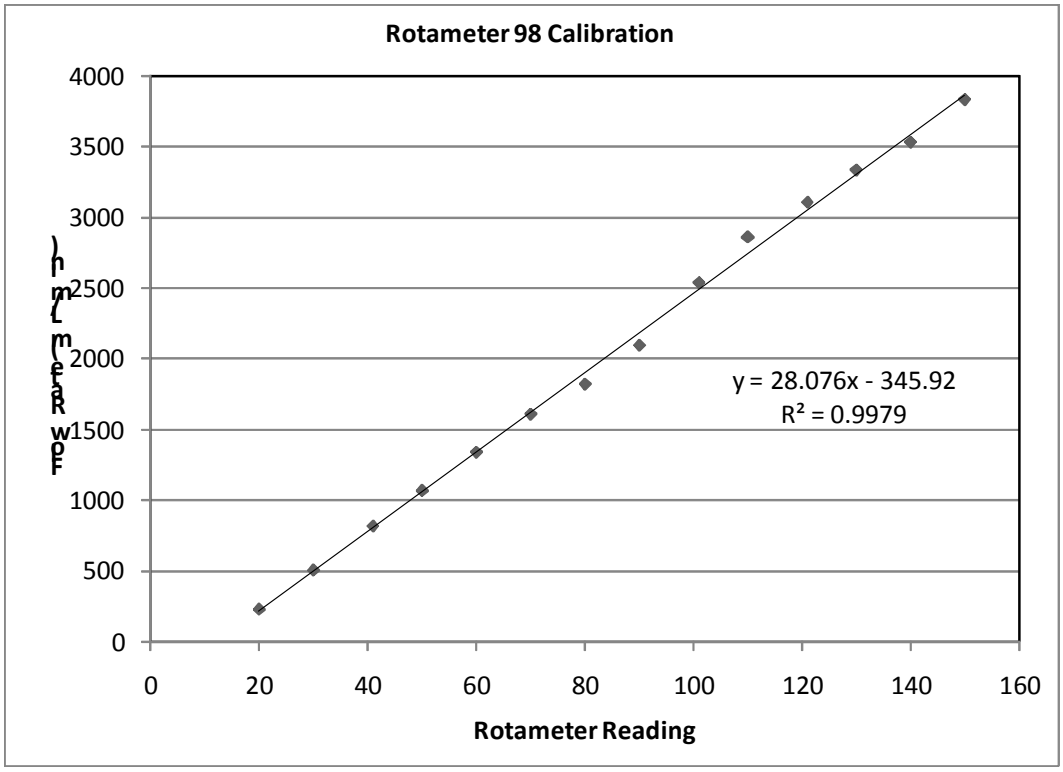

Figure B.1: Plot of flow rate v. rotameter reading for Rotameter 98.

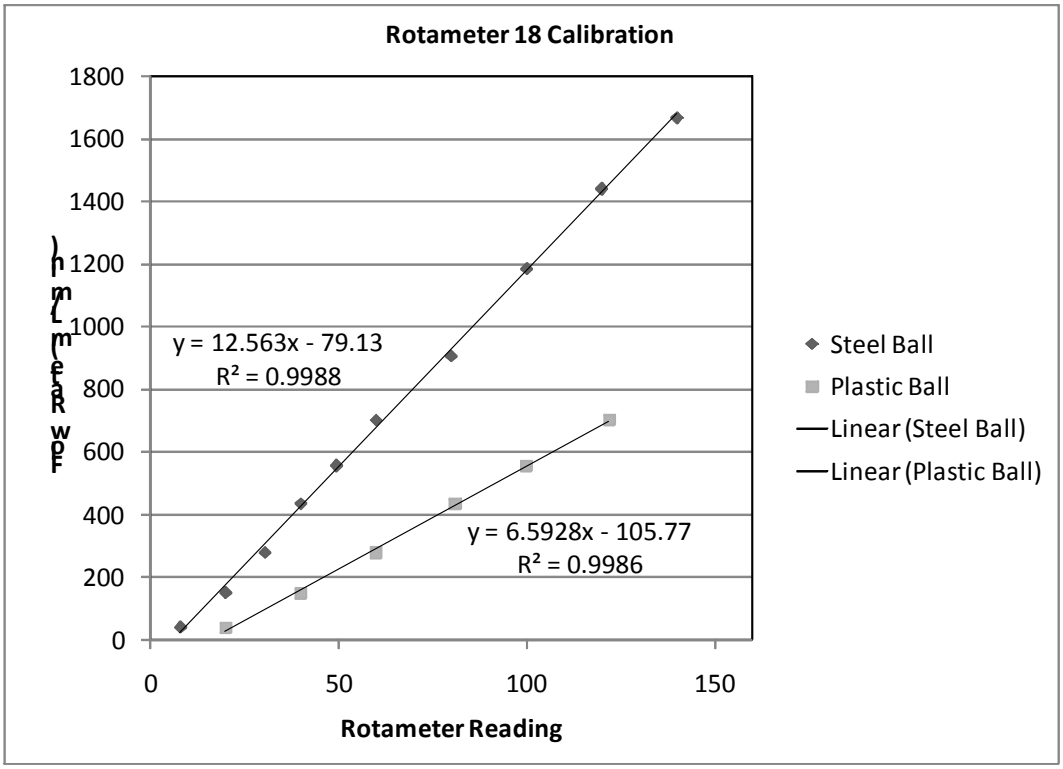

Figure B.2: Plot of flow rate v. rotameter reading for Rotameter 18.

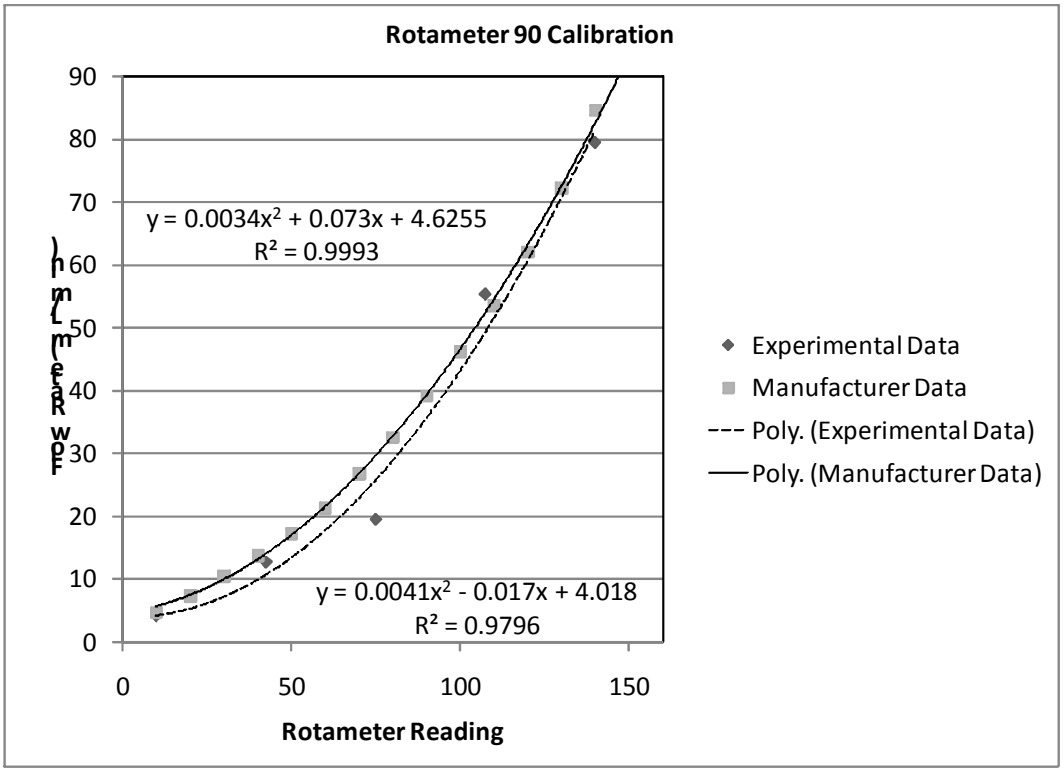

Figure B.3: Plot of flow rate v. rotameter reading for Rotameter 90.

B.2 GREEN TUBE FURNACE CALIBRATION

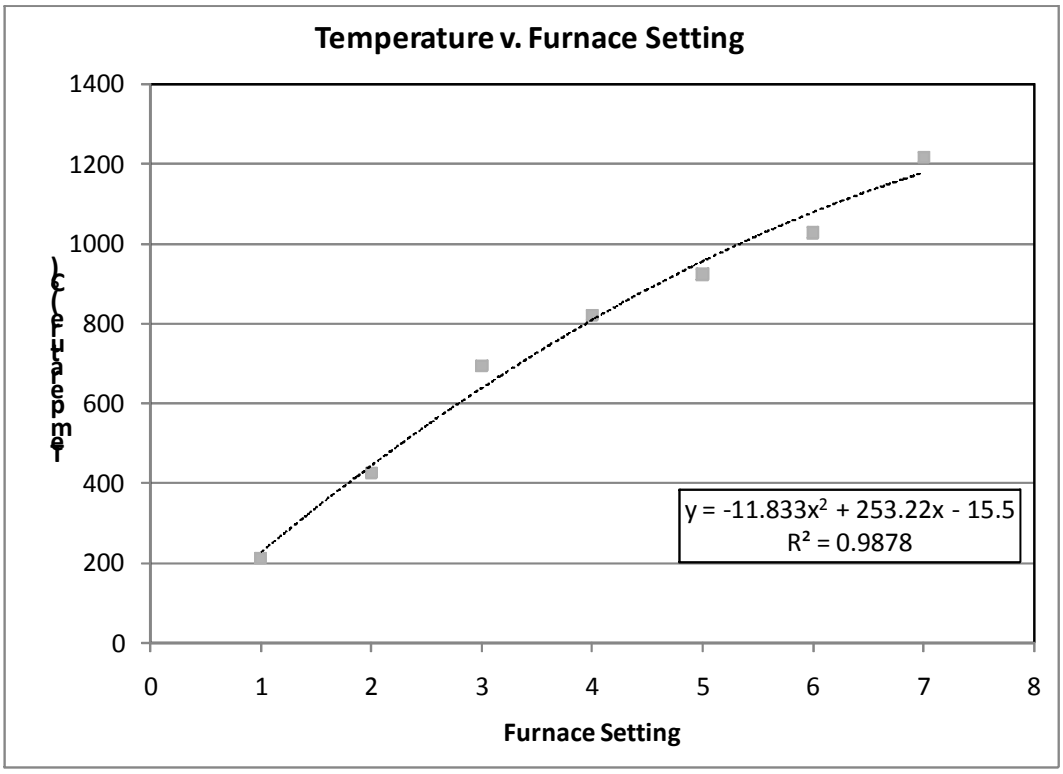

Figure B.4: Plot of thermocouple temperature v. furnace setting for the green analog furnace.

Appendix C: Uncertainty Analysis

The primary source of uncertainty in nanowire growth was temperature measurement. Flow rates were varied by 2 orders of magnitude with no repeatable effect on results so no uncertainty analysis of flow rates was done. According to Omega, the uncertainty on a K-type thermocouple is the greater of 2.2ºC or 0.75% (Omega Engineering, Inc. n.d.). The latter of these uncertainty specifications is greater for all the temperature ranges used in this research. The thermocouple error of the analog furnace is plotted in Figure C.1.

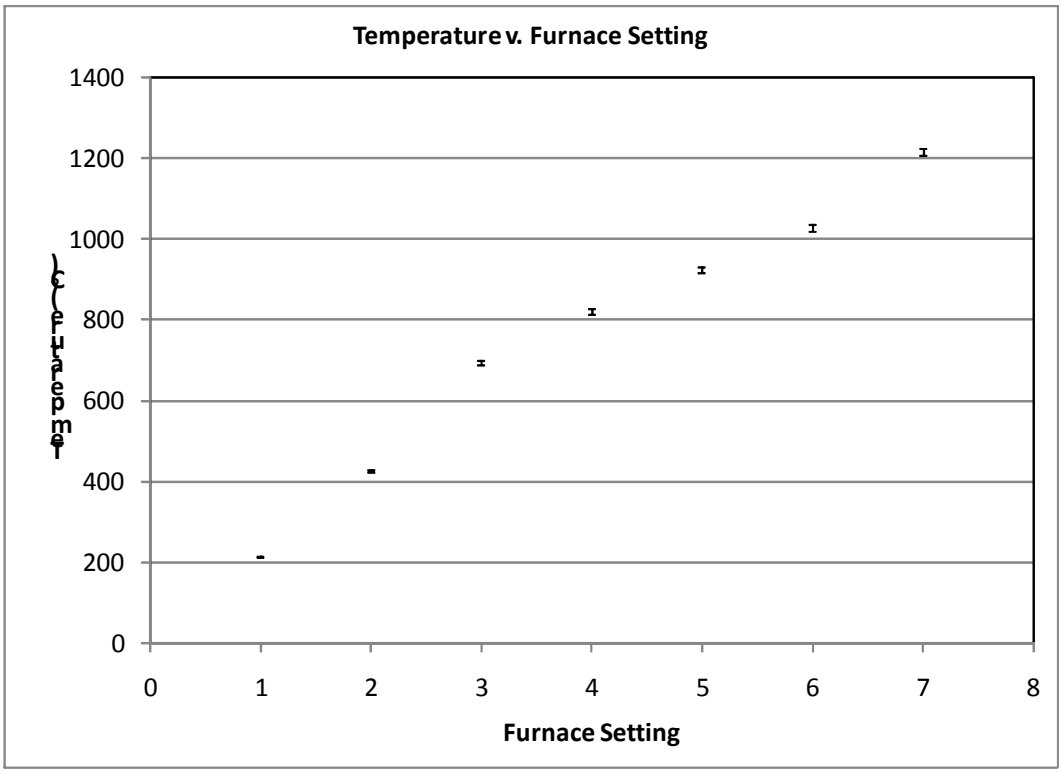

Figure C.1: Plot of temperature of analog tube furnace v. furnace setting with error bars. The error bars are small relative to the data range.

The thermocouple used to take the measurements presented in Figure C.1 was located in the very center of the quartz tube so it was measuring the temperature at which the quartz source material boat would be maintained.

There was also uncertainty in temperature due to spatial variations. The spatial temperature variation was measured with a K-type thermocouple for a downstream furnace set point of 800ºC and an upstream furnace setting of 6. The plot of these measurements with error for thermocouple uncertainty is shown in Figure C.2.

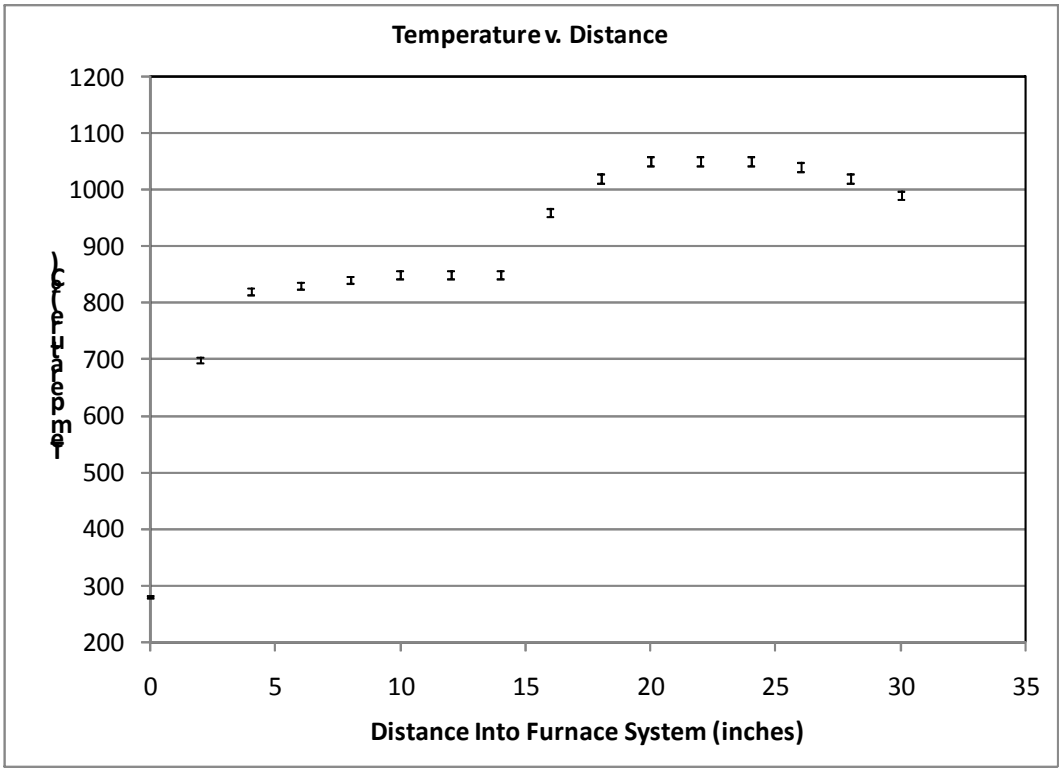

Figure C.2: Plot of temperature v. distance into furnace with thermocouple error. The error bars are small relative to the data range.

A plot of deviation from the set point for the digital furnace is shown in

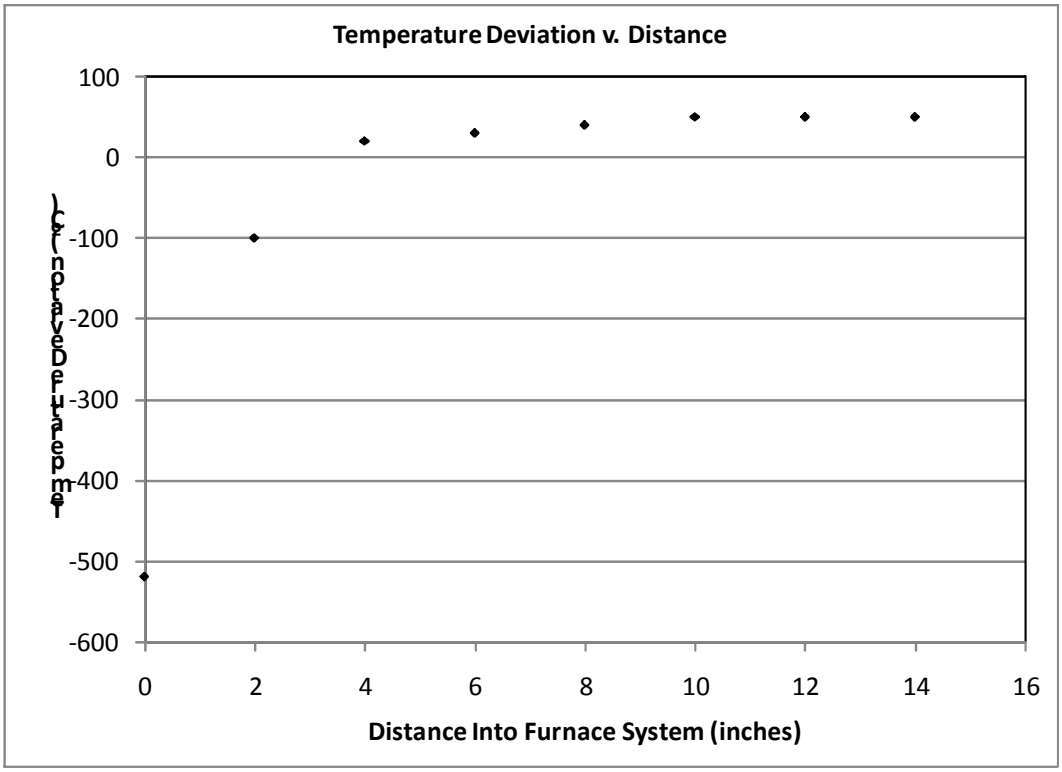

Figure C.3: Plot of temperature deviation from set point v. distance into furnace.

Bibliography

American Elements. *American Elements.* July 27, 2009. http://www.americanelements.com/zn.html#properties.

Buffat, Ph, and J-P Borel. "Size effect on the melting temperature of gold particles." *Physical Review A* 13, no. 6 (1976): 2287-2298.

Greene, Lori E., Benjamin D. Yuhas, Matt Law, David Zitoun, and Peidong Yang. "Solution-Grown Zinc Oxide Nanowires." (Inorganic Chemistry) 45, no. 19 (2006): 7535-7543.

Heck, Ronald M, and Robert J Farrauto. *Catalytic Air Pollution Control.* 2nd Edition. New York: John Wiley & Sons, Inc., 2002.

Hejazi, S R, Hosseini, and Ghamsari. "The role of reactants and droplet interfaces on nucleation and growth of ZnO nanorods synthesized by vapor-liquid-solid (VLS) mechanism." *Journal of Alloys and Compounds*, 2008: 353-357.

Huang, Michael H., Yiying Wu, Henning Feick, Ngan Tran, Eicke Weber, and Peidong Yang. "Catalytic Growth of Zinc Oxide Nanowires by Vapor Transport." (Advanced Materials) 13, no. 2 (2001): 113-116.

Kee, R. J., Michael Elliott Coltrin, and Peter Glarborg. *Chemically reacting flow: theory and practice.* John Wiley and Sons, 2003.

Kim, Dong Sik, Roland Scholz, Ulrich Gösele, and Margit Zacharias. "Gold at the root or at the Tip of ZnO Nanowires: A Model." (Small) 4, no. 10 (2008): 1615-1619.

Kirkham, Melanie, Xudong Wang, Zhong Lin Wang, and Robert L Snyder. "Solid Au nanoparticles as a catalyst for growing aligned ZnO nanowires: a new understanding of the vapor-liquid-solid process." (Nanotechnology) 18, no. 365304 (2007).

Kumar, R T Rajendra, et al. "Growth of ZnO nanostructures on Au-coated Si: Influence of growth temperature on growth mechanism and morphology." (Journal of Applied Physics) 104, no. 084309 (2008).

Li, Seu Yi, Chia Ying Lee, and Tseung Yuen Tseng. "Copper-catalyzed ZnO nanowires on silicon (1 0 0) grown by vapor-liquid-solid process." *Journal of Crystal Growth* 247 (2003): 357-362.

Okamoto, H. "Au-Zn (Gold-Zinc)." *Journal of Phase Equilibria and Diffusion* 27 (2006).

Omega Engineering, Inc. *Omega.com.* http://www.omega.com/techref/colorcodes.html (accessed July 15, 2009).

Pansare, Sourabh S., Amornmart Sirijaruphan, and James G. Goodwin Jr. "Au-catalyzed selective oxidation of CO: a steady-state isotopic transient kinetic study." *Journal of Catalysis* 234 (2005): 151-160.

Park, Joodong, Han-Ho Choi, Kerry Siebein, and Rajiv K. Singh. "Two-step evaporation process for formation of aligned zinc oxide nanowires." *Journal of Crystal Growth* 258 (2003): 342-348.

Prete, P, N Lovergine, and L Tapfer. "Nanostructure size evolution during Au-catalysed growth by carbo-thermal evaporation of well-aligned ZnO nanowires on (100)Si." *Applied Physics A* A 88 (2007): 21-26.

Rostedt, Mark G. MS Thesis, Austin, 2009.

Technical Glass Products. *Technical Information.* July 19, 2009. http://www.technicalglass.com/tech.htm#prop.

Tseng, Yung-Kuan, Hsu-Cheng Hsu, Wen-Feng Hsieh, Kuo-Shung Liu, and I-Cherng Chen. "Two-step oxygen injection process for growing ZnO nanorods." *Journal of Materials Research* 8, no. 12 (2003).

Unalan, Husnu Emrah, Pritesh Hiralal, Nalin Rupesinghe, Sharvari Dalal, William I Milne, and Gehan A J Amaratunga. "Rapid synthesis of aligned zinc oxide nanowires." *Nanotechnology* 19 (2008).

Voorhees, P W. "The theory of Ostwald Ripening." *Journal of Statistical Physics* 38, no. 1/2 (1985): 231-252.

Wang, Xudong, Jinhui Song, and Zhong Lin Wang. "Nanowire and nanobelt arrays of zinc oxide from synthesis to properties." (Journal of Materials Chemistry) 17 (2007): 711-720.

Wang, Zhong Lin. "Zinc oxide nanostructures: growth, properties, and applications." *Journal of Physics: Condensed Matter*, 2004: 829-858.

Yang, P D, et al. "Controlled Growth of ZnO Nanowires and Their Optical Properties." *Advanced Functional Materials* 12, no. No. 5 (May 2002).

Yao, B. D., Y. F. Chan, and N. Wang. "Formation of ZnO nanostructures by a simple way of thermal evaporation." (Applied Physics Letters) 81, no. 4 (2002).

Vita

Chad Allan Baker was born in Dallas, TX on July 3, 1983 to parents Allan and Debbie Baker. He was active in outdoor sports and Boy Scouts, earning the rank of Eagle Scout at age 17. He attended South Garland High School where he was involved in many extracurricular activities and graduated Salutatorian in a class of 482. Chad then attended Texas A&M University and earned a B.S. in Mechanical Engineering. Chad has passed the F.E. Exam to earn the title of Engineer in Training. He intends to continue his education to earn a Ph.D. in engineering, and he wants to do research in a faculty position at a university so that he may benefit humanity by improving technology and educating others.

Email: calbaker@gmail.com